# Suppressing cyanobacterial dominance by UV-LED TiO2-photocatalysis in a drinking water reservoir: a mesocosm study.

PESTANA, C.J., SANTOS, A.A., CAPELO-NETO, J. et al.

2022

# Suppressing cyanobacterial dominance by UV-LED $TiO_2$-photocatalysis in a drinking water reservoir: a mesocosm study

Carlos J. Pestana[a]*†, Allan A. Santos[b]*, José Capelo-Neto[c], Vânia M. M. Melo[d], Kelly C. Reis[c], Samylla Oliveira[c], Ricardo Rogers[b], Ana B.F. Pacheco[b], Jianing Hui[e], Nathan C. Skillen[f], Mário U.G. Barros[g], Christine Edwards[a], Sandra M.F.O. Azevedo[b], Peter K.J. Robertson[f], John T.S. Irvine[e], Linda A. Lawton[a]

* These two authors have contributed equally to the manuscript

† corresponding author: c.pestana@rgu.ac.uk

[a] School of Pharmacy and Life Sciences, Robert Gordon University, Aberdeen, UK

[b] Institute of Biophysics Carlos Chagas Filho, Federal University of Rio de Janeiro, Rio de Janeiro, Brazil

[c] Department of Hydraulic and Environmental Engineering, Federal University of Ceará, Fortaleza, Brazil

[d] Department of Biology, Federal University of Ceará, Fortaleza, Brazil

[e] School of Chemistry, University of St. Andrews, St. Andrews, UK

[f] School of Chemistry and Chemical Engineering, Queen's University Belfast, Belfast, UK

[g] Ceára Water Resources Management Company (COGERH), Fortaleza, Brazil

## Graphical Abstract

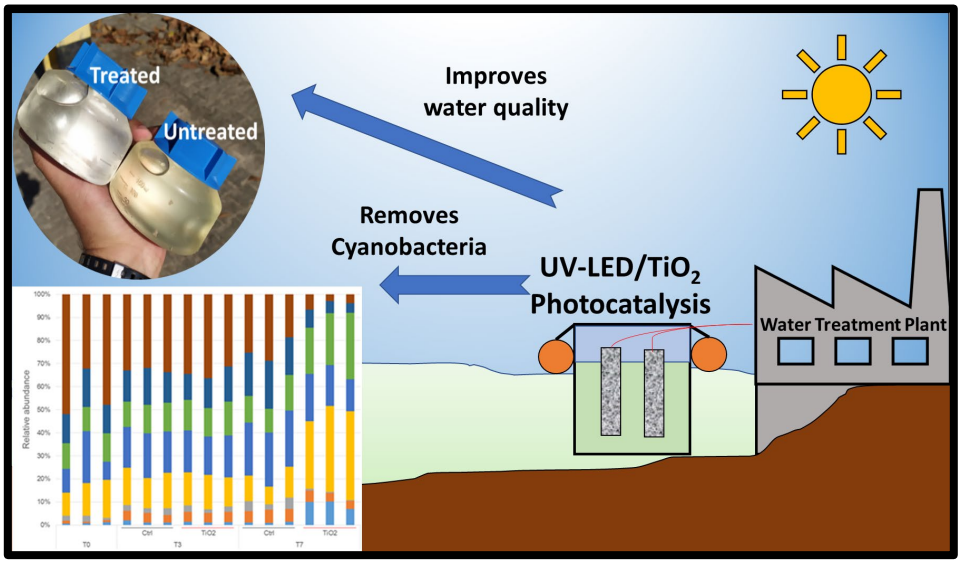


## Abstract

Cyanobacteria and their toxic secondary metabolites present challenges for water treatment globally. In this study we have assessed $TiO_2$ immobilized onto recycled foamed glass beads by a facile calcination method, combined in treatment units with 365 nm UV-LEDs. The treatment system was deployed in mesocosms within a eutrophic Brazilian drinking water reservoir. The treatment units were deployed for 7 days and suppressed cyanobacterial abundance by 85% while at the same time enhancing other water quality parameters; turbidity and transparency improved by 40 and 81% respectively. Genomic analysis of the microbiota in the treated mesocosms revealed that the composition of the cyanobacterial community was affected and the abundance of *Bacteroidetes* and *Proteobacteria* increased during cyanobacterial suppression. The effect of the treatment on zooplankton and other eukaryotes

was also monitored. The abundance of zooplankton decreased while *Chrysophyte* and *Alveolata* loadings increased. The results of this proof-of-concept study demonstrate the potential for full-scale, in-reservoir application of advanced oxidation processes as complementary water treatment processes.

**Keywords**: Phytoplankton; Advanced Oxidation Processes; Water quality; Microbial community; 16S/18S rRNA sequencing; Mesocosm

## Highlights

1) First *in situ* application of $TiO_2$-treatment units in a drinking water reservoir
2) $TiO_2$-based photocatalysis decreased *Cyanobacteria* abundance by 85% over seven days
3) Water quality improved significantly with higher transparency and lower turbidity
4) Good removal for potentially toxic *Raphidiopsis raciborskii* and *Microcystis* sp.
5) Treatment changed microbial dynamics contributing to *cyanobacterial* suppression

## 1 Introduction

Climate change and anthropogenically-driven (hyper)eutrophication of surface drinking waters lead to an increase in frequency and severity of cyanobacterial mass occurrence events called blooms (Paerl and Huisman, 2008).

Cyanobacterial blooms present significant challenges to the water treatment sector globally due to the potentially toxic cellular biomass in raw waters (Hitzfeld et al., 2000; Zamyadi et al., 2012). Modifying and upgrading existing infrastructure is often impractical and prohibitively costly. To counter the challenge posed by increased cyanobacterial blooms a paradigm shift to in-reservoir (pre-treatment) could be considered as an alternative treatment option. With targeted treatment of cyanobacteria and their toxins in the raw water prior to abstraction can ease the burden on existing water treatment plant (WTP) infrastructure. Promising technologies for in-reservoir pre-treatment include advanced oxidation processes (AOPs)*(Camacho-Muñoz* et al*.,* 2020*; Huang* et al., 2011; *Li* et al., 2017; *Menezes* et al., 2021). AOPs are chemical processes that generate highly reactive oxidative species (radicals) that can remove organic contaminants. The application of chemical oxidants as algaecides (e.g. $KMnO_4$, $H_2O_2$, $ClO_2$) has been explored previously with limited success *(Fan* et al., 2014, 2013). Usually, biomass removal occurs upon the application of chemical oxidants, which is desirable, however, the reduction in cell density goes hand in hand with the release of intracellular cyanotoxins.

A promising AOP for the removal of cyanobacterial cells and their toxins is semiconductor photocatalysis. $TiO_2$ is a semiconductor catalyst that upon incident of ultraviolet (UV) irradiation of <387 nm can generate hydroxyl ($\cdot OH^-$) and superoxide anion ($\cdot O_2^-$) radicals; via redox reactions on the surface of the photoexcited catalyst material in an aqueous matrix (Hoffmann et al., 1995). The removal of cyanobacteria and their toxins by $TiO_2$ nanoparticles has been previously documented (Lawton et al., 1999, 2003; Liu et al., 2003; Peter K.J.

Robertson et al., 1998). The deployment of nano-particulate $TiO_2$-photocatalysis in water treatment plants , to date, has been limited by the lack of validation of bench-scale studies at pilot and industrial scale (Loeb et al., 2019). The main underlying factors of the limited pilot/full scale evaluation have been designing and testing of suitable photocatalytic treatment units that move the technology readiness level (TRL) up the scale. In the current study, we have made progress addressing the technology transfer from bench-scale testing towards implantation of the technology for water treatment by immobilizing $TiO_2$ nanoparticles onto beads made from foamed, recycled glass and using a low energy, waterproof UV-LED lighting system for deployment at mesocosm scale. In previous studies we have demonstrated the efficacy of the $TiO_2$-coated beads in controlling cyanobacteria and their toxins at bench scale (*Gunaratne* et al., 2020; *Pestana* et al., 2020c, 2020a) and at pilot scale (*Menezes* et al., 2021). This investigation evaluates the removal of cyanobacteria in a mesocosm study within an operating drinking water reservoir in the Northeast of Brazil that suffers from perennial cyanobacterial blooms. Our previous work, evaluation of $H_2O_2$ treatment of cyanobacteria, in this reservoir demonstrated the suitability of the constructed mesocosms and the study site to examine water treatment *in situ* (Santos et al., 2021). The current study sets out to evaluate:

- the efficiency of photocatalytic removal of cyanobacteria,
- the effect of treatment systems on physico-chemical water quality parameters,
- and the effect on non-target species of the microbial community

## 2 Material and Methods

### 2.1 $TiO_2$-coated glass bead production and photocatalytic reactor construction

Glass beads made from foamed recycled glass (2-4 mm diameter; Dennert Poraver, Germany) were coated with $TiO_2$ according to a method described previously (Gunaratne et al., 2020; Pestana et al., 2020c). In short, acetone washed glass beads were repeatedly added to a $TiO_2$ slurry (0.1 g $mL^{-1}$ P25 $TiO_2$ nanoparticulate powder [Degussa Evonik, Germany] in ultrapure water with 1 drop 5 $mL^{-1}$ KD6 dispersant [Croda, UK]) and calcinated at 500 °C for 1 h until a w/w ratio of 10% $TiO_2$ was achieved (with each coating step depositing ~ 2% w/w), followed by a final calcination step at 500 °C for 10 h. Coated beads were washed with ultrapure water to remove fines, dried at 100 °C, and stored until used.

The photocatalytic reactors were constructed from stainless-steel wire mesh with an aperture size of 1.2x1.2 mm and a wire thickness of 0.4 mm. The outer reactor consisted of a 1000x80 mm wire cylinder. Along the inside length of the mesh cylinder five aluminum profiles were attached with stainless-steel screws (Fig 1c). Each profile housed a 1000 mm length of waterproof UV-LEDs (LightingWill, UK; 365-370 nm; IP68 rated, 4.8 W $m^{-1}$, 120 LEDs $m^{-1}$). Each set of five LED strips were powered by an AC/DC adapter that delivered 12 dcV and ~ 3A. The power output was 8.32 W $m^{-2}$ on average. Tetrahedral wire mesh pods (18; made from the same wire mesh as the outer reactor) containing 8 g of $TiO_2$-coated glass beads each were placed inside the wire mesh cylinder. Reactors were capped, top and bottom, with 80 mm diameter

wire mesh disks. Waterproof connectors were used to supply a mains power line which was run from onshore.

## 2.2 Experimental Site and Mesocosm set-up

The current study was conducted in the Gavião Reservoir (3°59'03''S/38°37'13''W), a drinking water system located in a semi-arid area in the Northeast of Brazil; that presents a high solar radiation reaching about 5 kWh $m^{-2}$ $day^{-1}$, 8 hours per day, and an average atmospheric temperature of 32 ºC (FUNCEME, 2017; Barros et al., 2019). Gavião Reservoir is known for perennial cyanobacterial blooms (Barros et al., 2019). In general, the is eutrophic, presenting an average depth of 10 m in the lacustrine zone, with a water storage capacity of 3.3 x $10^7$ $m^3$ in a hydraulic basin of 618 hectares and a water retention time of about 22 days on average (Barros et al., 2019; Santos et al., 2021). The study was carried out in October-November 2019 with an average air temperature of 28 °C (maximum: 32 °C), and < 0.1 mm precipitation according to the National Institute of Meteorology - INMET (INMET - National Institute of Meteorology (Brazil), 2019; Table S1). Six mesocosms were constructed, consisting of a cylindrically shaped bag (1.5 m diameter and 2 m depth) of impermeable and semi-transparent plastic which was supported and kept afloat by a PVC (polyvinyl chloride) tube structure. The mesocosms were tethered to a floating platform which housed the electronic components for the photocatalytic reactors, located close to the WTP intake point. The bottom of the mesocosm was completely sealed, separating the water inside from the reservoir (Figure 1). All mesocosms were filled with approximately

3000 L of reservoir water. The controls were tree mesocosms with no photocatalysis and three which housed the LED-powered-$TiO_2$ reactors (Figure 1).

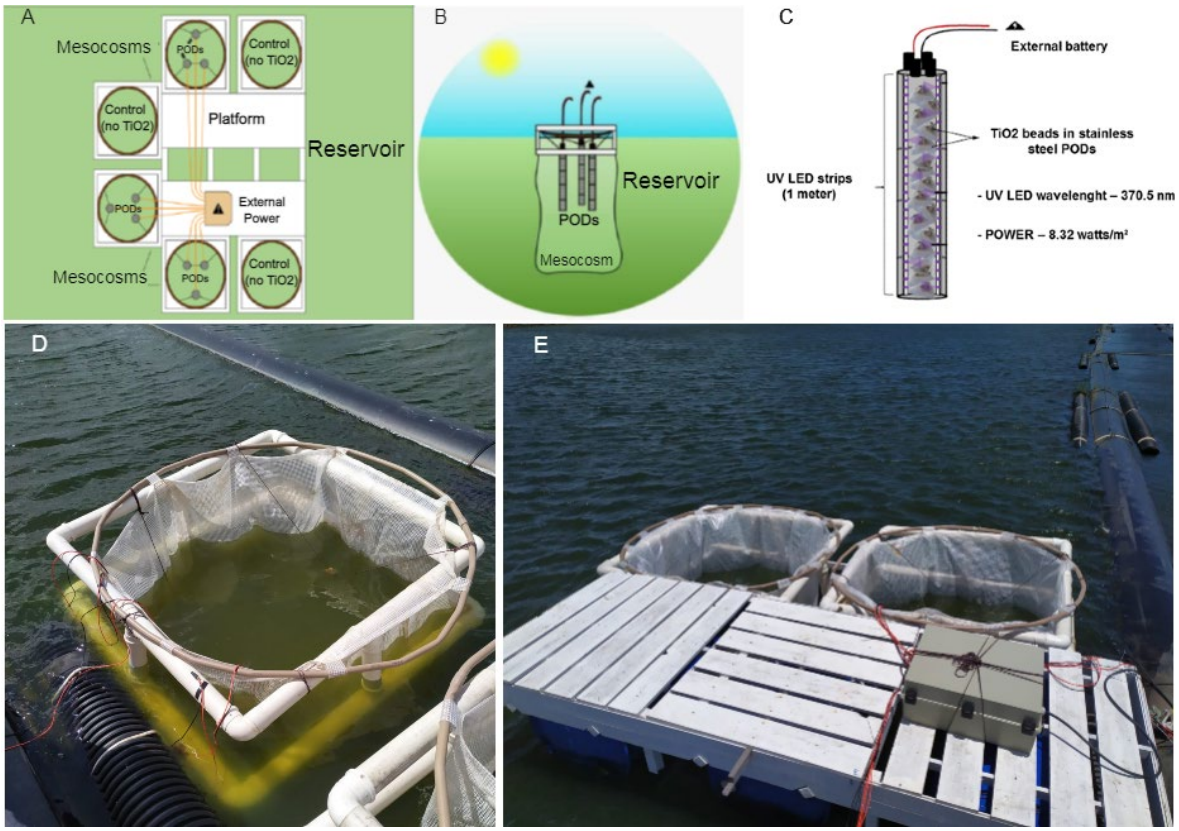


**Figure 1:** Mesocosm deployment in Gavião reservoir October-November 2019. (A) Illustration of the platform containing three mesocosms for each condition (with and without $TiO_2$ reactors. (B) mesocosm with $TiO_2$-coated beads in stainless-steel pods. (C) Reactor design. (D) Mesocosm *in situ*. (E) Mesocosms with external power supply for LEDs.

## 2.3 Sampling and monitoring analyses

For each sampling time (0, 3 and 7 days), abiotic and biotic parameters were analyzed (Table S2). Composite samples were collected with a 1800x50 mm long PVC pipe and tight-fitting rubber bung by placing the pipe in the center of the mesocosm and submerging it the entire depth of the mesocosm; it was

then capped with the rubber bung and the sample was removed and placed into amber glass bottles that were stored at 4 °C until laboratory analysis. To obtain the microbial community, 500 mL of water was filtered through 0.22 µm SteritopTM filter units (Merck Millipore®, Massachusetts, US). The material retained on the filters was used for DNA extraction.

### 2.4 DNA extraction, amplification and high-throughput sequencing

Membrane filters containing cells were cut into pieces with sterile surgical blades and used to extract DNA with the cetyl trimethylammonium bromide (CTAB)-based method, that uses a cationic detergent to disrupt cells. The procedure was performed according to Winnepenninckx et al. (1993). The concentration and quality of DNA preparations were verified with a Nanodrop ND-1000 spectrophotometer (Thermo Scientific, Waltham, MA, USA). The V4 region of the 16S rRNA gene and the V9 region of the 18S rRNA gene were targeted to determine the composition of the bacterial and eukaryotic plankton communities. The respective set of primers was 515F/806R (F515 - 5′ GTGCCAGCMGCCGCGGTAA 3′ and R806 - 5′ GGACTACHVGGGTWTCTAAT 3′) for Bacteria (Caporaso et al., 2011) and Euk1391f/EukBr (Euk 1391f - 5′ TATCGCCGTTCGGTACACACCGCCCGTC 3′) and EukBr - 5′ AGTCAGTCAGCATGATCCTTCTGCAGGTTCACCTAC 3′) for Eukarya (Amaral-Zettler et al., 2009). The first amplification, incorporating barcodes in the forward primer, was performed using the following program: 95 °C for 4 min, 60 °C for 1 min, 72 °C for 2 min, followed by 25 cycles at 94 °C for 1 min, 60 °C for 1 min, and 72 °C for 2 min. Each sample was marked with a specific

barcode so that it could be recognized after high-throughput sequencing. The resulting amplicons were purified using calibrated Ampure XP beads (Beckman Coulter, Indianapolis, IN, USA) according to the manufacturer's instructions. All samples were subjected to a second PCR to incorporate dual indices as described in the 16S and 18S Metagenomic Sequencing Library Preparation Protocol for the Illumina MiSeq system (San Diego, California, US). Final amplicons were paired-end sequenced using an Illumina MiSeq Reagent Kit v2 (500 cycles, 2 × 250 bp) on an Illumina MiSeq sequencer (Illumina, San Diego, CA, USA).

### 2.5 Data acquisition and processing

After sequencing, Illumina adapter sequences were trimmed from already-demultiplexed raw fastq files using Cutadapt v1.8 (Martin, 2011) in paired-end mode, and the reads quality were assessed using FastQC v.0.11.8 (Andrews, 2010) and vsearch v2.10.4 (Rognes et al., 2016). Subsequent analyses were performed in the R v3.5.3 environment (R Core Team, 2020), following the DADA2 v1.11.1 package (Callahan et al., 2016) pipeline to obtain a table of non-chimeric amplicon sequence variants (ASVs; sequences differing by as little as one nucleotide) (Callahan et al., 2017). Taxonomy assignment and removal of non-bacterial sequences was performed against the SILVA reference database (release 138, December 2019) (Callahan, 2018; Yilmaz et al., 2014), whereas the assignment for eukaryotic community was performed using the PR2 reference database (Guillou et al., 2013). The 16S and 18S rRNA data were deposited in the NCBI Bioproject database with accession no.

PRJNA754369 and PRJNA754602, respectively (https://www.ncbi.nlm.nih.gov/bioproject).

### 2.6 Statistical analysis

For a detailed description of the statistical analysis please refer to the supplementary material (S2.2). In short, for the abiotic factors principal component analysis (PCA) followed by Shapiro-Wilk determination ($p<0.05$) and a Wilcoxon-Mann-Whitney test to determine significant differences in relevant parameters between treatment and control was carried out. Statistical analyses for abiotic factors were performed using R software version 3.4.1, using the Factoshiny package (Vaissie et al., 2020).

For biotic factors (bacterial and eukaryotic plankton communities), we performed a linear discriminant analysis (LDA) and effect Size (LEfSe) (Segata et al., 2011) (the Hutlab Galaxy web framework - http://huttenhower.sph.harvard.edu/galaxy/) to select significant biomarker taxa ($p<0.05$) between treatment and control over time (at genus level) using LDA score of 3.5 as threshold ($log_{10}$ transformed).

From the 18S rRNA data, we used the taxonomic groups identified and gathered the main taxa (>3% relative abundance in at least one sample) in relevant freshwater plankton groups, following the classification described in previous studies (Cavalier-Smith, 2018; Simpson and Eglit, 2016; Table S2).

The beta-diversity ordination was evaluated by nMDS (non-metric dimensional scaling) considering ASVs abundance in a tridimensional space using the Bray-Curtis distance as dissimilarity matrix, which was complemented by

permutational multivariate analysis of variance (two-way PERMANOVA) using two factor groups, condition (control and treatment) and time ($p<0.05$). To test the correlation between abiotic and biotic (ASVs-based taxa) factors and differences in the community structure over time, the samples were ordained by Canonical Correspondence Analysis (CCA) using the Hellinger-transformed abundance matrix and Spearman analysis ($p<0.05$ and a threshold for r value =±0.4). The analyses were performed, and charts plotted in R v3.5.3 environment (R Core Team, 2020) and Past3 software (Hammer et al., 2001).

## 3. Results and Discussion

### 3.1 Effect of $TiO_2$ photocatalysis on cyanobacteria and raw water quality

The $TiO_2$-based photocatalysis treatment system placed in mesocosms in a eutrophic reservoir in Brazil significantly affected bacterioplankton dynamics when compared to the control ($p=0.001$ $F=3.90$) over time ($p=0.0001$ $F=8.25$) according to PERMANOVA analysis. nMDS ordination provides a clear distribution opposing control and treatment conditions, mainly for the day 7 (Figure S1).

Following treatment using $TiO_2$ photocatalysis the relative abundance of the cyanobacteria decreased in the treatment mesocosms compared to the control mesocosms (figure 2).

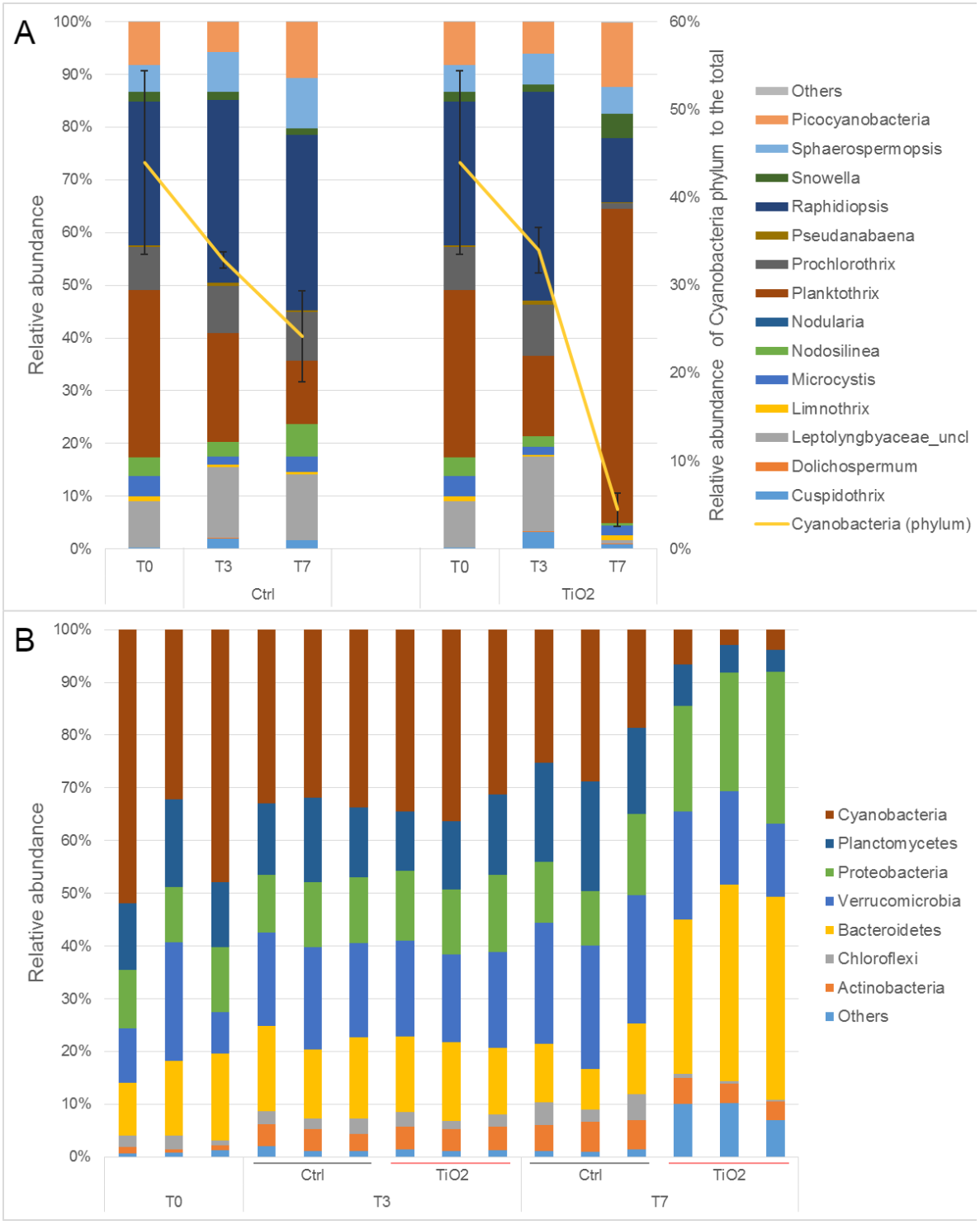


**Figure 2:** Relative abundance of cyanobacteria in the treatment and control condition over time determined by 16S rRNA sequencing (A) and dynamics in the relative abundance of the phyla in the bacterioplankton over time also determined by 16S rRNA sequencing (B). In (A), the secondary axis shows the relative abundance of the cyanobacteria phylum in relation to the entire bacterioplankton community (yellow line, grouping the mean and standard deviation). The bars resulted from triplicate samples (n=3). In (B) the effect of $TiO_2$-based photocatalysis (red $TiO_2$) on the main phyla of the bacterioplankton community compared to the untreated control (black

Ctrl) is shown. Data from triplicate samples for both conditions (n=3). Taxa designated as "others" are described in Table S4.

Initially, the bacterioplankton composition was dominated by *Cyanobacteria*, with 45% relative abundance on average, and members of *Bacteroidetes*, *Verrucomicrobia*, *Planctomycetes* and *Proteobacteria* contributed as major other phyla (Figure 2B). After three days, the relative abundance of cyanobacteria decreased to about 33-35% (Figure 2 and Table S3). The most pronounced effect of the treatment was observed on day 7, when the cyanobacterial contribution decreased to less than 5%, on average, in the mesocosms where the photocatalytic units had been deployed, while it represented approximately 25% in the control. This selective removal of cyanobacteria by ROS-based treatment methods has been described previously and is linked to the internal structure of cyanobacteria and the co-action of irradiation-induced intracellular ROS generation (Drábková et al., 2007). Specifically, the photosynthetic apparatus in cyanobacteria is not segregated into organelles and has direct connection with the plasma membrane of the cell, thus making it more susceptible to ROS attack (Grossman et al., 1995) and the cyanobacterial light-harvesting complex (the phycobilisome) is located outside of the thylakoidal membrane thus, making it more susceptible to external ROS attack (Grossman et al., 1995). Cyanobacteria have also been shown to be sensitive to ROS attack due to having a limited enzymatic defense mechanism lacking the common ROS-eliminating ascorbate peroxidase (Passardi et al., 2007) and most species further lacking alternative members of the haem peroxidase family of ROS-defense enzymes (Bernroitner et al.,

307 2009). Further, it has been shown that irradiation-induced intercellular
308 generation of ROS by the Mehler reaction can overwhelm the internal
309 enzymatic ROS defense mechanisms under increased irradiation levels such a
310 those presented by the UV-irradiation provided by the photocatalytic reactors
311 in the current study (Tytler et al., 1984). Additionally, it has been
312 demonstrated that the phycocyanin pigment, which is unique to cyanobacteria,
313 can enhance photocatalytically-generated ROS attacks (Robertson et al.,
314 1998). The combination of these effects is responsible for the selective
315 sensitivity of cyanobacteria to the proposed treatment system.
316 *Planctomycetes* abundance also decreased following photocatalytic treatment
317 compared to controls. In contrast, *Bacteroidetes* increased its abundance from
318 14% in the control to 35%, on average, following photocatalytic treatment and
319 *Proteobacteria* increased in abundance from 12% in the control condition to
320 24% with photocatalytic treatment (Figure 2 and Table S3).
321 Using different loadings of $TiO_2$ nanoparticles (15, 100, and 1000 mg $L^{-1}$) in
322 samples from three different Swedish lakes, Farkas et al. (2015) observed a
323 high impact on the bacterial community in a dose dependent manner,
324 considering their abundance and activity, which was estimated by the
325 incorporation of radioactive labeled L-[4,5-$^3$H]-leucine. They also reported that
326 the light regime considering the UV and PAR (photosynthetically active
327 radiation) sources compared to the dark condition contributed to the decrease
328 on bacterial activity mainly from the highest concentration of $TiO_2$
329 nanoparticles. Moreover, the authors observed that $TiO_2$ effects on bacterial
330 abundance and activity were stronger in lakes with high dissolved organic

carbon (DOC) and low chemical elements concentrations; however, they did not investigate any modification on bacterioplankton composition.

In our findings, LEfSe analysis identified the most important taxa considering cyanobacteria and non-cyanobacteria that contributed to the differential abundance between treatment and control ($p < 0.05$) (Figure S2). Using a LDA threshold of 3.5, we selected 38 genera that reflected the effect of $TiO_2$ on the $7^{th}$ day, including 18 resistant and 20 susceptible taxa.

We observed that the main susceptible organisms, besides cyanobacteria, were unclassified taxa from *Phycisphaeraceae* (CL500_3), and *Methylacidiphilaceae* families, *Sphingobacteriales* order as well as the genus *Terrimicrobium* compared to the control condition (Figure 3A-D). The resistant taxa, *Flectobacillus*, *Asinibacterium*, *Prosthecobacter* and *Armatimonas* contributed to about 60% of the bacterioplankton community in the treatment mesocosms (Figure 3E-H).

The application of $TiO_2$ photocatalysis represents a continuous low-level treatment with a steady production of reactive oxigen species (ROS) compared to the addition of oxidants (e.g., hydrogen peroxide) that are dosed at a set concentration with an (almost) immediate, albeit short-lived effect. This is clearly demonstrated when comparing our previous study (Santos et al., 2021) investigating the application of hydrogen peroxide in mesocosms to the current one. In this study, photocatalytic treatment showed a marked decrease in the

355 cyanobacterial phytoplankton portion between days 3 and 7 of the treatment
356 compared to a marked decrease for cyanobacteria after 24 h for the hydrogen
357 peroxide study conducted in the same reservoir. Apart from *Cyanobacteria*,
358 other susceptible taxa were identified as heterotrophic members of the
359 *Phycisphaeraceae* family (*Planctomycetes*), this appears reasonable as this
360 family has been described as directly related with cyanobacterial taxa in
361 marine (*Synechococcus*) and freshwater systems (*Microcystis*) (Chun et al.,
362 2019; Zheng et al., 2020), explaining their simultaneous decrease in relative
363 abundance (Figure 3).
364
365

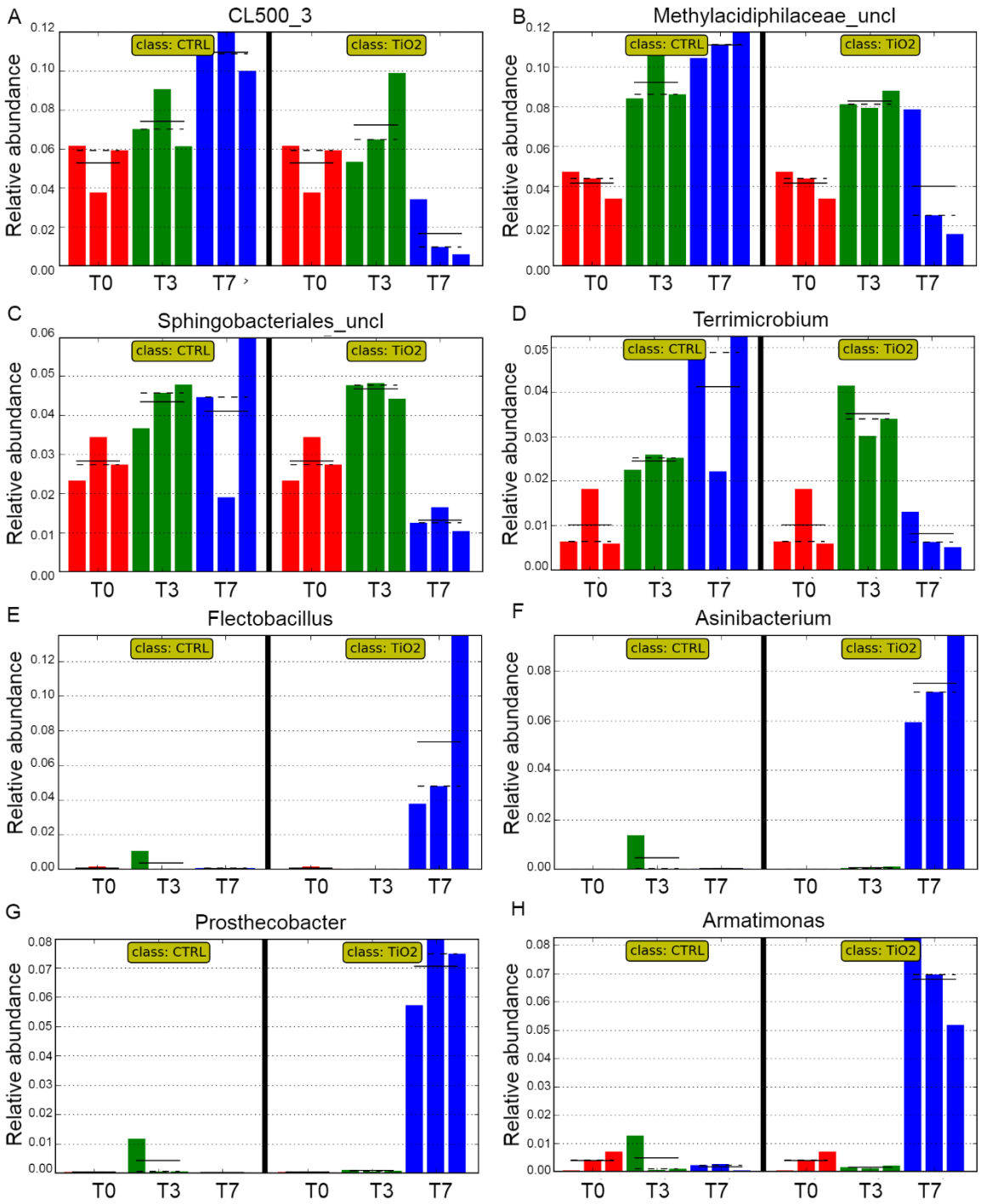


**Figure 3:** Differential abundance of heterotrophic bacterial taxa affected by $TiO_2$ compared to the control condition according to LEfSe analysis ($p < 0.05$), considering sensitive (A-D) and resistant organisms (E-H). The different colors express the sampling days T0 (red), T3 (green) and T7 (blue) from the triplicate samples. Full black lines represent the average of three samples, the dashed black line represents the median.

374 Additionally, *Terrimicrobium* (*Terrimicrobiaceae*) identified in the current study
375 as susceptible to the treatment process was also identified as vulnerable after
376 $H_2O_2$ treatment in this same reservoir (Santos et al., 2021).
377 *Flectobacillus*, *Asinibacterium*, *Prosthecobacter* and *Armatimonas* were
378 identified as resistant taxa in the current study (figure 3E-H) increasing in
379 relative abundance as the cyanobacterial (and other susceptible taxa)
380 abundance decreased in the treatment mesocosms.
381
382 Reasons for resistance against ROS attack could be an increased production of
383 carotenoids, as observed by Asker et al. (2012) for *Flectobacillus* in a
384 radioactively impacted region in Japan. Asker et al. (2012) and others
385 (Martínez-Laborda et al., 1990; Stafsnes et al., 2010) proposed that
386 carotenoids were able to quench ROS produced by UV-irradiation and photo-
387 oxidation. Besides the production of pigments such as high carotenoid
388 contents, the protection against ROS may be due to the efficient enzymatic
389 activities for reducing the oxidative damage (Slade and Radman, 2011; Takebe
390 et al., 2007). The resistance/tolerance to ROS-attack allows taxa to capitalize
391 on resource availability or reduced competition (Litchman et al., 2015)
392 explaining the marked increase of the aforementioned resistant taxa in the
393 treatment mesocosms.
394
395 As mentioned earlier, *Cyanobacteria* dominated both bacterioplankton and
396 phytoplankton which was also observed by other authors for the same and
397 similar reservoirs (Dokulil and Teubner, 2000; Guedes et al., 2018; Liu et al.,

2019). Focusing on the genus level, 40 genera were observed consisting of *Cyanobacteria* (18), *Chlorophyta* (11), *Bacillariophyta* (5), *Charophyta* (3), *Euglenozoa* (2), *Cryptophyta* (1) and *Ochrophyta* (1) (Table S6). *Cyanobacteria* reached approximately 98% of the total phytoplankton with a density of around $10^6$ cell $mL^{-1}$ in both control and treatment conditions. The composition of the observed cyanobacteria genera, originally composed mainly of *Planktothrix agardhii*, *Raphidiopsis raciborskii*, *Pseudoanabaena sp.* and *Pseudolyngbya sp.,* was modified by the treatment. Within the cyanobacteria grouping, a dominance of *Planktothrix* and *Raphidiopsis* in the original community (32% and 28%, respectively) (Figure 2A) was observed. Additionally, <10% Picocyanobacteria (including *Cyanobium*, *Synechococcus* and *Synechocystis*), *Sphaeropermopsis*, *Prochlorothrix*, *Microcystis* and an unclassified genus of *Leptolyngbyaceae* (Figure 2A) were detected.

On day 3 of the experiment, *Raphidiopsis* presented a higher abundance than at T0 while *Planktothrix* decreased in abundance in both conditions. Following the decrease of cyanobacterial abundance by the 7$^{th}$ day, *Planktothrix* (61%) presented the highest relative contribution of cyanobacteria compared to the other sampling times and to the control. We also detected a higher resistance of *Planktothrix* compared to the other *Cyanobacteria* genera (Figure 2A). Santos et al. (2021) monitored cyanobacteria by pigment fluorescence and the bacterioplankton composition (16S rRNA sequencing) after applying 10 mg $L^{-1}$ $H_2O_2$ to a mesocosm system in the same drinking water reservoir. *Cyanobacteria*, originally composed of *Planktothrix sp*., *Raphidiopsis sp*.,

*Microcystis sp*. and *Cyanobium sp*., were suppressed for 5 days after a single application of $H_2O_2$. Non-filamentous cyanobacteria were most resistant against $H_2O_2$, while *Planktothrix* sp. was markedly affected throughout the treatment; interestingly unlike the results presented here. Thus, in both mesocosm studies *Planktothrix* sp. and *Raphidiopsis* sp. dominated the initial cyanobacterial community but although both $H_2O_2$ and $TiO_2$/UV produce ROS, they affected the cyanobacterial community differently.

However, there is no clear evidence that supports different pattern of interspecific resistance/sensitivity, mainly for *Raphidiopsis* sp. and *Planktothrix* sp. considering specific ROS. For treatment purposes this aspect should be further explored since both cyanobacterial genera have shown a co-dominance (along with *Dolichospermum* sp.) in drinking water reservoirs, mainly in the Brazilian semi-arid region (Barros et al., 2019; Clemente et al., 2020; Pestana et al., 2019; Santos et al., 2021). Interestingly, in $H_2O_2$ studies at lab scale, (Yang et al., 2018) evidenced similar values for effective concentration ($EC_{50}$) of $H_2O_2$ that inhibit the growth of *Planktothrix* (0.42 mg $L^{-1}$) and *Raphidiopsis* (0.32 mg $L^{-1}$) as well as damage to the photosynthetic apparatus, whereas non-filamentous *Microcystis* presented higher resistance.

The diverse composition of other cyanobacterial taxa and the bacterioplankton community in each case may have affected the different outcomes in terms of competitive or synergistic interactions and succession.

More detailed information on the genomics data is provided in the Supplementary Information (Figures S2 and S3, as well as Tables S4 and S5).

Physico-chemical parameters representing water quality markedly improved over the course of the study in the treated mesocosms versus the control mesocosms (table 1).

**Table 1:** Effect of $TiO_2$-based photocatalysis on selected water quality parameters in mesocosms located within a drinking water reservoir. Data from triplicate samples for both conditions.

| Parameters | Raw water (T0) | 3 days | | 7 days | |
|---|---|---|---|---|---|
| | | Treated | Control | Treated | Control |
| **Transparency (cm)** | 51 ± 2.7 | 96 ± 3 | 52 ± 5 | 96 ±18 | 53 ± 3 |
| **Turbidity (TU)** | 6.76 ± 0.25 | 3.83 ± 0.42 | 6.04 ± 0.18 | 2.37 ± 0.77 | 4 ± 0.52 |
| **True Colour (HU)** | 69.5 ± 6.6 | 68.2 ± 10.9 | 72.1 ± 7.8 | 98.3 ± 44.6 | 85.8 ± 14.2 |
| **pH** | 8.85 ± 0.16 | 9.63 ± 0.17 | 9.73 ± 0.21 | 8.22 ± 0.13 | 8.61 ± 0.12 |
| **Organic Matter ($UV_{254nm}$)** | 0.261 ± 0.01 | 0.252 ± 0.01 | 0.261 ± 0.01 | 0.261 ± 0.02 | 0.261 ± 0.01 |
| **Total Organic Carbon (mg $L^{-1}$)** | 21.57 ± 3.07 | 17.73 ± 0.85 | 21.57 ± 1.91 | 15.27 ± 0.38 | 18.33 ± 0.93 |
| **Dissolved Organic Carbon (mg $L^{-1}$)** | 14.57 ± 1.16 | 16.63 ± 0.91 | 16.8 ± 3.07 | 14.4 ± 0.72 | 17.07 ± 1.46 |
| **Dissolved oxygen (mg $L^{-1}$)** | 7.32 ±1.53 | 3.21 ± 1.13 | 6.17 ± 0.19 | 3.07 ± 1.19 | 6.17 ± 0.1 |

Transparency almost doubled on average in the treatment mesocosms, while turbidity practically halved, which is logical as both parameters are inversely related. This observation was confirmed by PCA analysis which identified pH, total and dissolved organic carbon (TOC and DOC), dissolved oxygen, turbidity, and transparency as the most relevant physico-chemical variables (Figure S3). The pH was directly proportional to the variables TOC and DOC. The highest values of transparency were associated with the lowest values of turbidity and dissolved oxygen.

462 This trend for turbidity and transparency was also observed in our previous
463 study with solar irradiation and hydrogen peroxide (10 mg $L^{-1}$) applied in the
464 same reservoir (Santos et al., 2021). Increased transparency represents an
465 improvement in the water quality both for treatment purposes and from an
466 ecological perspective. The fact that the $TiO_2$-photocatalysis applied here
467 reduced the turbidity and increased the transparency means it improved its
468 own performances for the treatment purposes. Its effective capability for these
469 physical aspects should be emphasized sinceorganic particles initially competed
470 with bacteria for ROS and for the photoactive sites of the $TiO_2$. Furthermore,
471 suspended particles reduced light penetration through the water by dispersion.
472 By reducing these effects, the treatment became more effective, which could
473 be a possible explanation for the lag time in observable effects of the
474 treatment on the phytoplankton communities before day 7. Ecologically,
475 greater transparency means light can penetrate deeper into the water column
476 thus expanding the euphotic zone and generating oxygen in deeper zone of the
477 reservoir. Additionally, eukaryotic phytoplankton can take better advantage of
478 light penetration growing faster and bringing new stability to the water system.
479
480 A reduction of the dissolved oxygen concentration was observed throughout
481 the experiment, which may have been caused by two mechanisms: the action
482 of the oxidative process promoted in the treatment reactors and the water
483 retention inside the mesocosms. The latter reduces the mixing processes of the
484 water column, thus influencing its stratification (Båmstedt and Larsson, 2018).
485 The depth of the mesocosms in the current study (1.5 m), is comparable to

shallow areas within reservoirs or reservoirs that experience water shortage and are only fractionally filled. This, combined with the fact that the experiment took place during the time of  year with traditionally high temperatures, the current mesocosm design could favor weak thermal stratification inside the system comparable to most reservoirs in the Brazilian semi-arid region (Marques et al., 2019).

Regarding the DOC concentration, values remained close to the control at T0 and day 3 with no major changes observed. The concentrations of TOC followed a similar trend as that observed for DOC. TOC results showed little significant differences in most experimental times after exposure to the photocatalysis.

There was no modification of nutrient or salt ion concentrations over time, as would be expected (supplementary information S4, Table S6, Figure S4). The continuing presence of nutrients could theoretically favor regrowth of the cyanobacteria, which is why it is important to bear in mind that the current system is designed to be continually operating and treating the reservoir, it is not designed to prevent the formation of blooms by nutrient-control, but by population-control.

### 3.2 Effect of $TiO_2$ photocatalysis on the eukaryotic plankton community

Combined with the marked effects on the bacterioplankton community in the reservoir the $TiO_2$/UV treatment significantly affected the eukaryotic plankton

community in general (p=0.0049 F=3.21 according to PERMANOVA when compared to the control) over time (p=0.0001 F=6.73), especially for the zooplankton community.

nMDS ordination provides a clear distribution opposing control and treatment conditions, mainly for the day 7 (Figure S1). While little change was observed at day 3, on day 7 of the treatment the zooplankton community decreased from around 61% of the total eukaryotic plankton community to less than 5% (Figure 4).

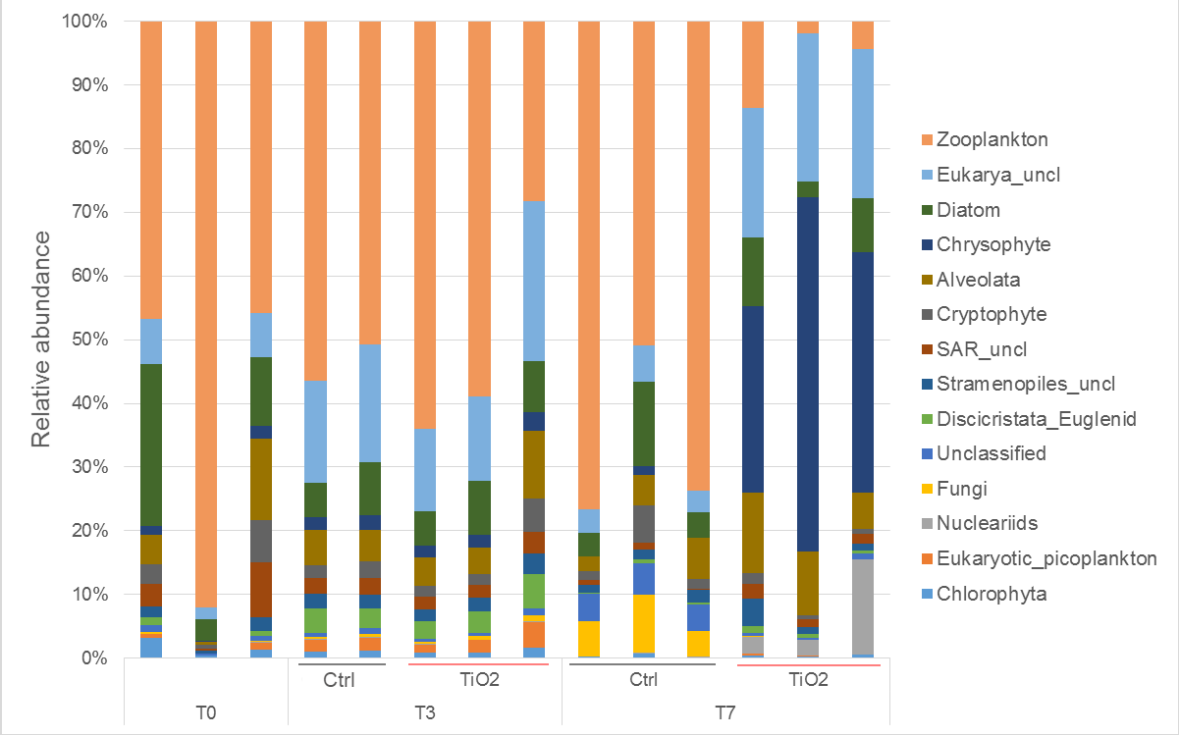


**Figure 4:** Effect of $TiO_2$-based photocatalysis on eukaryotic plankton community showing the taxonomic composition with the relative abundance of the main planktonic groups. The main taxa identified after sequencing (>3% of relative abundance in at least one sample) were grouped in relevant freshwater planktonic groups. Data from triplicate samples for both conditions (n=3), except for the control condition at day 3, in which one replicate was removed due to the low number of sequences recovered.

Originally, the community was rich in zooplankton, followed by the diatom and alveolate groups, which together accounted for over 75% of the eukaryotic plankton community (Figure 4). The *Arthropoda* subclass *Copepoda* was the main component of zooplankton, accounting for 50% on average (Table S7), with *Calanoida* and *Cyclopoida* as the main taxa in this group (Table S3). Diatoms contributed ~13% of the total eukaryotic plankton community including *Fragilariales* as the major group (10% of Diatom). Alveolate represented ~6% of the total eukaryotic plankton community with *Dinoflagellata* as the main representative (4% of Alveolate) (Figure 4, Table S7). On day 3, there was no clear evidence of compositional changes except for an increase in the abundance of an unclassified member of Eukarya and a decrease in the diatom group (to 7% on average), although this occurred in both conditions (Figure 4 and Table S7).

On day 7 the relative abundance of zooplankton decreased by more than 95% on average (Figure 4 and Table S7) whereas *Chrysophyte* increased to about 41% compared to its low abundance at the start of the experiment and in the control condition on day 7 (0.5%-1%). The decrease in the relative abundance of zooplankton components may be a direct effect of the oxidizing treatment or a secondary effect due to changes in the phytoplankton community composition, mainly linked to the modification of cyanobacterial dynamics where *Planktothrix* dominated the cyanobacteria community compared to the original distribution at T0 and the control condition, where *Raphidiopsis,* *Pseudoanabaena* and *Pseudolyngbya* were more prevalent (Figure 2A).

Different zooplankton species have different preferred target food species (Tõnno et al., 2016); however, it stands to reason that in a biome that is so strongly dominated by cyanobacteria as is the current study site, a large portion of the zooplankton grazes on cyanobacteria as preferred food source. Thus, a possible explanation of the marked decrease of the zooplankton abundancy is that due to the reduction of cyanobacterial abundance an important food-source for zooplankton was removed leading to the zooplankton reduction. A detailed investigation of the zooplankton species present in the reservoir and an investigation of their feeding behavior would clarify these possibilities but was out with the scope of the current study.

Within *Chrysophyte*, the taxa *Chromulinales* (12%), *Chrysophyceae* (10%) and *Ochromonadales* (19%) family/order presented the highest increase in contribution (Table S6), suggesting resistance to the treatment. Interestingly, the *Chrysophyte* also referred to as golden-brown algae, presented an increase in the treated mesocosms which is unlikely as was observed for the effect of $H_2O_2$ in different studies; where the treatment promoted the growth of green algae when applied to mitigate cyanobacterial blooms (Fan et al., 2019; Santos et al., 2021; Yang et al., 2018).

An unclassified member of Eukarya increased to 22% in the treatment compared to < 5% in the control condition. Although less abundant, alveolate also increased in abundance at this time. Members of the family *Perkinsidae*

reached about 8% of relative contribution compared to T0 or the control condition (~1%) (Table S7).

Following this pronounced modification on day 7, LEfSe analysis identified the most important eukaryote taxa contributing to the observed effect ($p < 0.05$) (Figure S2B). Using the LDA 3.5 threshold, we detected a lower number of taxa that distinguished the $TiO_2$ based photocatalysis treatment and the control condition, where resistant and susceptible components included 11 and 8 taxa, respectively.

Besides *Calanoida* and *Cyclopoida* organisms, we observed the zooplankton *Ploimida* (*Rotifera*) and the fungi *Catenaria* (*Blastocladyales*) as susceptible organisms (Figure 5A-D). These four taxa represented about 60% of the original eukaryote community, which was considerably diminished on day 7.

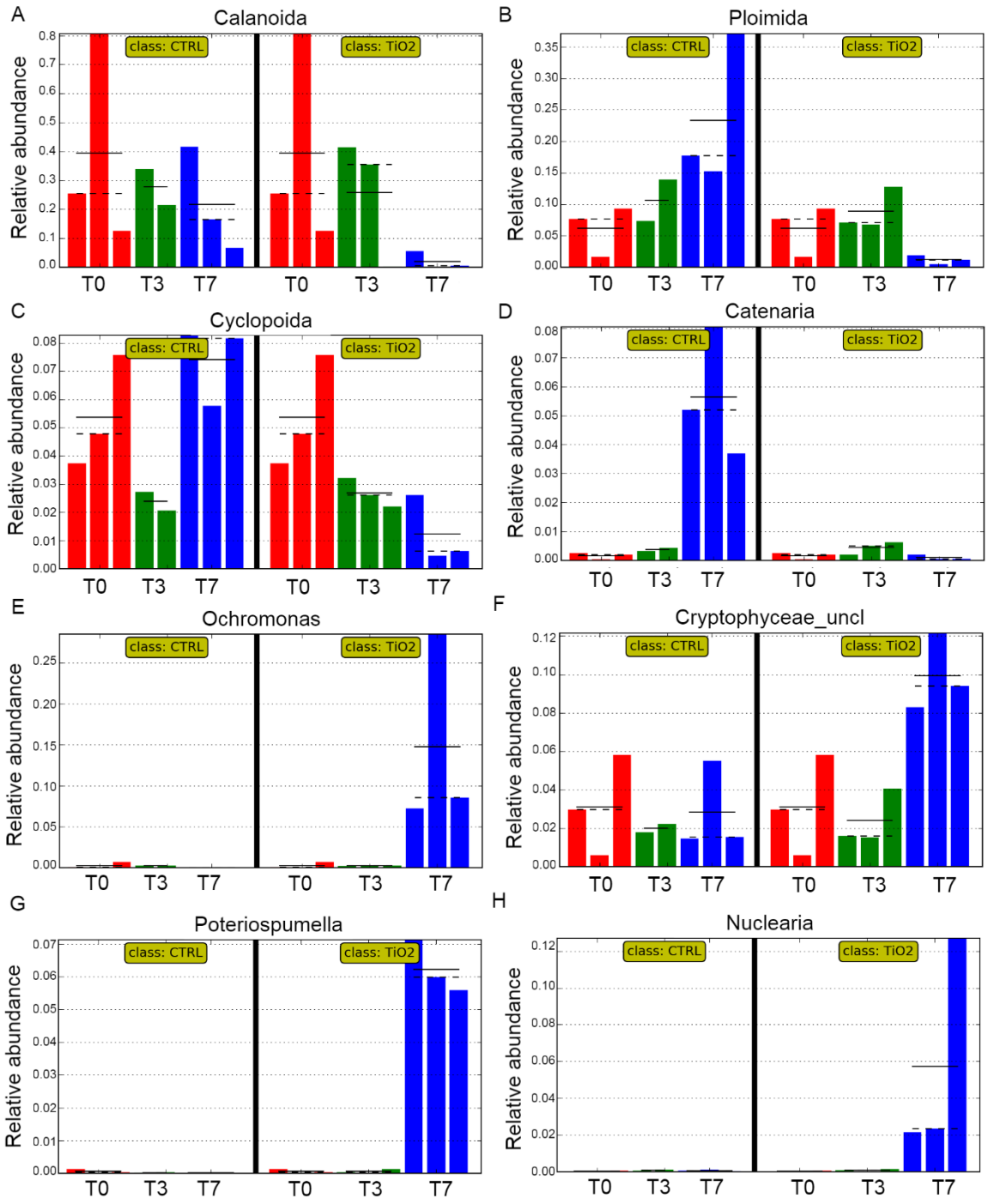


589
590 **Figure 5:** Differential abundance of eukaryote taxa affected by $TiO_2$ compared to the
591 control condition according to LEfSe analysis ($p < 0.05$), considering susceptible (A-D)
592 and resistant organisms (E-H). The different colors express the sampling days T0
593 (red), T3 (green) and T7 (blue). Data are represented as means of triplicates except
594 for T3, as those samples presented a very low number of sequences. Full black lines
595 represent the average of three samples, the dashed black line represents the median.
596

597

598 In the resistant group, with the highest LDA scores in the $TiO_2$ treatment, we
599 identified *Ochromonas* (*Ochrophyta*), *Chrysophyceae_uncl* (unclassified),
600 *Poteriospumella* (*Chrysophyte*) and *Nuclearia* (*Gastrotricha*) (Figure 5E-H and
601 Figure S2B). *Ochromonas*, *Poteriospumella* and *Nuclearia* did not present
602 significant abundance at any sampling time, except for day 7 of the treatment
603 condition, when their abundances rose to 15% and 6-7%, respectively,
604 indicating a resistance to the $TiO_2$-based photocatalysis (Figure 5E, G and H,
605 respectively).
606
607 Following that, *Poteriospumella* and *Ochromonas* genera from the *Chrysophyte*
608 were the most relevant taxa to increase in abundance throughout the
609 photocatalytic treatment. The antioxidant activity from both *Chrysophyte*
610 genera is unclear and any report that could explain this specific response
611 against ROS could not be found. However, it is known that other *Chrysophyte*
612 species from marine environment present a pronounced ability to produce
613 lipopolysaccharide and carotenoids, such as fucoxanthin, which produces a
614 high antioxidant response, considering both ROS quenching as well as photo-
615 damage protection (Méresse et al., 2020; Sun et al., 2014). The increased
616 abundance of this group in the treatment conditions may be linked to an
617 intrinsic resistance or can reflect the impact on the microbial plankton
618 community composition, including the decrease of the originally dominant
619 cyanobacteria and zooplankton. Also, these organisms could have taken
620 advantage of the altered abiotic environmental conditions that occurred as a
621 result of the treatment, e.g., increased light availability due to a decrease in

622 turbidity and increase in transparency. Although these organisms are
623 mixotrophic, they present a pronounced heterotrophy activity with limited use
624 of light as energy source (Graupner et al., 2018). For example, in North
625 America lakes, *Chrysophyte* species are commonly found in oligo- and
626 mesotrophic environments where their competitive ability in phosphorous
627 limitation allows them to dominate the planktonic community over other algae
628 (Nicholls and Wujek, 2003). Although we did not observe any change in
629 nutrient content, this group could dominate the eukaryote community due to
630 other factors besides microbial composition, such as DOC dynamics, their
631 mixotrophic characteristics, as well as the increased light availability in the
632 photocatalytic system.
633
634 Interestingly, *Ochromonas* have been identified as *Microcystis* grazers and a
635 microcystin (cyanotoxin) degrader after an ultrasound-assisted process was
636 used at lab scale to estimate its application for water cleaning and
637 cyanobacteria controlling (Zhang et al., 2021, 2018). Alternatively, the
638 treatment could stimulate an indirect control of cyanobacteria and a potential
639 microcystin degradation by promoting an increase in Ochromonas abundance.
640 This fact indicates the importance of investigating the ecological role of
641 microbial communities resistant to alternative treatments and their capacity for
642 degrading diverse toxic compounds that may be released after treatment.
643
644
645

### 3.3 Relationship between biotic and abiotic parameters

In this study, we tested for correlation between relevant abiotic parameters affected by the treatment and selected taxa, corresponding to the susceptible or resistant bacterial and eukaryotic taxa (high LDA scores according to the LEfSe analysis at T7) including the main cyanobacterial genera observed in 16S rRNA data. We used a canonical correspondence analysis (CCA) coupled to Spearman correlation ($p<0.05$) (Figure 6 and Table S8).

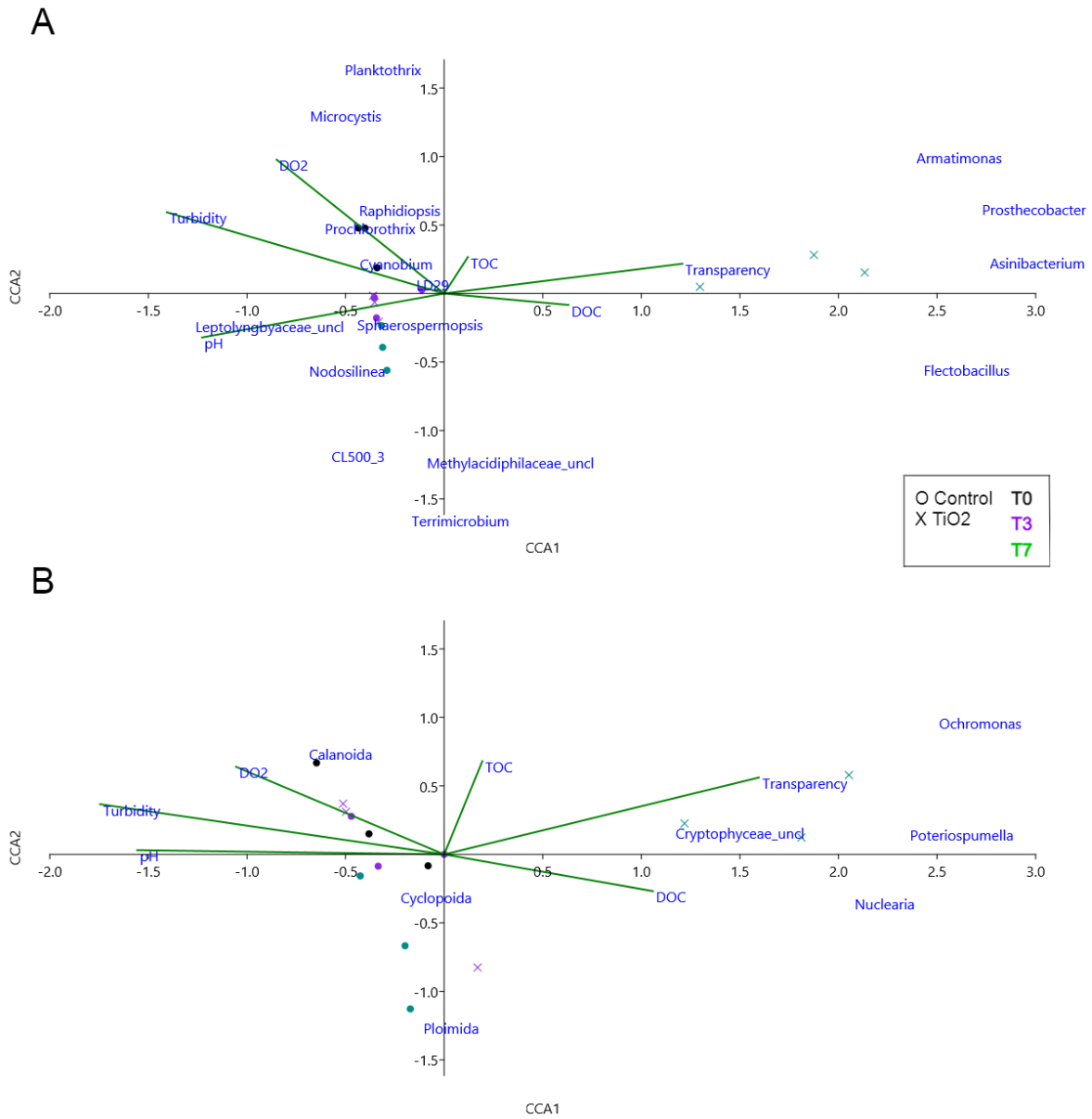


**Figure 6:** Canonical correspondence analysis (CCA) considering the relevant physico-chemical parameters affected by the treatment over time and the main susceptible and resistant genera from the bacterial (A) and eukaryotic (B) plankton communities. Taxa used as input here were from sequencing data that contributed to the differentiation between control and treatment according to the highest LDA scores from LEfSe analysis ($p < 0.05$).

For the bacterioplankton, the CCA ordination had the total variation of data explained by the two main axes (82 and 14%, respectively) with a significant p-value for their eigenvalues (p=0.01 and 0.02, respectively).

A strict relationship was observed between turbidity and all cyanobacterial genera sharing the same dimensional quadrant, which considered all sampling times for the control condition, including T0 (Figure 6A), in which cyanobacteria maintained high relative abundance. This was confirmed by the Spearman analysis, showing a significant positive correlation between turbidity and cyanobacteria with high r-values for *Planktothrix* and *Microcystis* (r=0.67 for both) as well as *Raphidiopsis* and *Sphaerospermospsis* (r=0.54 for both) (Table S8). For transparency, *Microcystis* presented a significant negative correlation (r=0.61), as well as *Cyanobium* and *Nodosilinea* (r= -0.60 and -0.66, respectively). The resistant bacteria *Asinibacterium* and *Prosthecobacter* presented significant negative correlations with turbidity (r= -0.74 and -0.45, respectively) and a positive correlation with transparency (r=0.57 and 0.44, respectively).

The association between cyanobacterial dynamics and the improvement of turbidity and transparency was previously observed from the use of $H_2O_2$ in Gavião reservoir (Santos et al., 2021) where the chlorophyll content of these organisms decreased over time simultaneously with an increase in transparency.

Other abiotic parameters such as dissolved oxygen and pH also presented a positive correlation with susceptible cyanobacterial genera and negative correlations with resistant bacteria. For dissolved oxygen the correlation was significant for *Microcystis* (r= 0.51), *Planktothrix* (r= 0.50) and

689 *Sphaerospermopsis* (r= 0.53) and for the resistant *Asinibacterium* (r= -0.55)
690 and *Prosthecobacter* (r= -0.46). For pH, significant correlations were found for
691 the cyanobacteria *Leptolyngbyaceae_uncl*: (r= 0.68), *Prochlorothrix* (r= 0.50)
692 and *Raphidiopsis* (r= 0.44) and for the resistant taxa Flectobacillus (r= 0.51)
693 (Figure 6A and Table S7).
694
695 Organic carbon content (TOC and DOC) presented negative correlation with the
696 cyanobacteria *Cyanobium* and *Microcystis* (r=0.45 and 0.53, respectively) and
697 with the heterotrophic bacteria CL500_3 and LD29 (r=0.47 and 0.58,
698 respectively), whereas *Prosthecobacter*, a resistant bacterium, showed positive
699 correlation with TOC and DOC (r=0.61 and 0.49, respectively; Table S8). This
700 relationship between TOC/DOC and bacteria, among cyanobacteria and
701 heterotrophic ones, could be associated to the photodegradation and lysis of
702 susceptible cyanobacteria while other bacteria could be involved in the
703 biodegradation of intracellular products released to the water (Huang et al.,
704 2017; Ye et al., 2015). Farkas et al. (2015) observed a strict relationship
705 between the $TiO_2$ nanoparticles and organic carbon affecting the bacterial
706 community, where lakes with higher concentrations of DOC and lower chemical
707 element concentrations presented a significant reduction of bacterial
708 abundance and activity. Although we identified a positive correlation between
709 some resistant taxa (among bacteria and eukaryote) and DOC, we could not
710 establish the influence of carbon on the treatment efficiency.
711

712 In the eukaryotic community, CCA showed a discrete ordination of taxa and
713 abiotic parameters with fewer relationships when compared to the
714 bacterioplankton (Figure 6B). The two main axes explained the total variation
715 of data, contributing with 69 and 21%, respectively, and significant p-values
716 (p=0.002 and 0.1, respectively).
717
718 *Cyclopoida* was the only susceptible taxon located opposite transparency
719 topresent a negative correlation with this parameter (r= -0.54). In contrast,
720 the resistant *Ochromonas*, *Poteriospumella* and *Nuclearia* were located close to
721 transparency, in the opposite quadrant (Figure 6B). *Ochromonas* (r=0.58) and
722 *Nuclearia* (r=0.55) were positively correlated with transparency, whereas
723 *Poteriospumella* was negatively correlated with turbidity (r=-0.44).
724 *Ochromonas* and *Nuclearia* also showed positive correlation with TOC and DOC
725 (r=0.47 and 0.58, respectively, for *Ochromonas* and r=0.55 and 0.53,
726 respectively, for *Nuclearia*) (Table S8).
727

728 ### 3.4 *In situ* application of $TiO_2$-based photocatalysis

729 For over twenty five years, the potential of $TiO_2$ photocatalysis as a promising
730 technology for the control of cyanobacteria and their toxins has been described
731 in the literature (Lawton et al., 1999; Robertson et al., 1997; Robertson et al.,
732 1998). Much of the work, however, has involved lab scale applications with
733 only a small number of reports detailing pilot scale reactor studies (Menezes et
734 al., 2021; Pestana et al., 2014). Consequently, much of the work reported has
735 been at lower Technology Readiness Levels (TRLs) between 1 and 3. To move

this technology further up the TRL scale, larger scale applications capable of treating cubic meter quantities of water, will need to be demonstrated. In this paper, for the first time, the technology has been demonstrated to be a feasible *in situ* treatment step capable of larger scale water treatment hence moving the photocatalytic process up the TRL scale from four to five. It is envisioned that, continuous or as-needed-treatment with the proposed system adjacent to the WTP abstraction point could ease the cyanobacterial burden on the treatment plant. The removal of cyanobacteria and the intrinsic improvement of water quality could significantly decrease the need for treatment chemicals which is economically and environmentally favorable. The exact number of treatment units required would be determined on a case-by-case basis dependent on local conditions and incoming raw water quality/cyanobacterial load. Considerations of the potential inherent cost of the deployment system can be found in the Supplementary information (S8). Previous work has clearly demonstrated that the proposed technology can remove both cyanobacteria and dissolved cyanotoxins (Gunaratne et al., 2020; Pestana et al., 2020c). This markedly decreases the public health dangers posed by toxic cyanobacterial blooms and could potentially also mitigate the effects of cyanobacteriogenic taste and odor episodes, as the removal of taste and odor compounds by $TiO_2$ photocatalysis has described before (Pestana et al., 2014, 2020b).

Post-treatment testing has demonstrated that the coating on the beads is stable (Figure S5 and S6). It was observed that iron and manganese were incorporated into the elemental composition of the $TiO_2$-coated beads, which is

most likely from components of the treatment unit. The photocatalytic efficiency of the used beads was tested against methylene blue in the laboratory (Figure S7) and a 20% drop in removal efficiency was observed, most likely due to the aforementioned contamination with Fe and Mn. For future iterations of this treatment system, materials will have to be carefully selected to avoid affecting the photocatalytic efficiency.

In the current study, we observed alterations in the phyto- and zooplankton communities as a result of the photocatalytic treatment. Whether any changes would affect the microbial community in a water body the size of a drinking water reservoir would have to be carefully examined in due course. It is worth bearing in mind, however, that any type of intervention (e.g., limiting nutrient input or application of broad-spectrum algaecides) will have a knock-on effect on the micro-biosphere of a water body and will have to be carefully evaluated to balance the desired effects. A potential additional area of concern is the effect of the treatment on disinfection by-product formation. The effect of the $TiO_2$-photocatalysis in this regard will have to be carefully monitored and coordinated with carefully dialed-in treatment conditions in the disinfection step. Furthermore, as the treatment solution presented here is designed to be operated continuously the danger of re-growth of undesirable species is low compared to periodic treatments such as the application of algaecides or $H_2O_2$.

In the future, it would be desirable to power the lighting array with renewable energy systems such as photovoltaic or wind power depending on the local

784 climatic conditions. A promising approach would be the deployment of floating
785 photovoltaic units that feed a battery system, allowing for 24-hour operation of
786 the photocatalytic units. An additional advantage of the application of floating
787 photovoltaic units would be the shading of the underlying water, further
788 limiting cyanobacterial growth. Although the environmental impact of the use
789 of photovoltaic units would have to be assessed against the benefits of their
790 employment (Farrell et al., 2020). The application of the treatment units is not
791 limited to the reservoir alone. While it is envisaged that this will be the main
792 deployment point, deployment in settling tanks or on top of filter units within
793 the conventional water treatment unit processes could unlock further potential
794 to polish water and decrease treatment costs by increasing filter-life and
795 decreasing the demand for chemical disinfection.
796

797 **4. Conclusion**

798 To ultimately ease the burden on water treatment plants an innovative $TiO_2$-UV
799 LED reactor system was tested at mesocosm scale. Within seven days
800 cyanobacterial abundance was reduced by 85% and water quality parameters
801 like transparency and turbidity improved markedly. The current study
802 represents a move towards bridging the gap between decades of academic
803 laboratory-based research towards real life deployment of the technology,
804 pushing the TRL further up the scale.
805 The proposed photocatalytic system aims to be sustainable with readily
806 available and recycled constituent parts. Off-the-shelve components were used
807 to construct the reactor system complimented by a facile photocatalyst

deposition method onto beads made from post-consumer glass. While the treatment units were powered by mains power in the current study, there is scope to utilize renewable energy systems to further enhance the sustainability aspect.

Due to the flexibility the system offers (reactor length could be increased or decreased as required) other applications can be envisaged including deployment on top of filters within conventional water treatment plants as well as a polishing technology of product water and within product water storage. Areas for future research include full lake trials, long-term effect on the ecosystem, life cycle analysis and techno-economic assessment to further push the treatment system up the TRL scale.

To conclude, we have, for the first time, demonstrated practical application of $TiO_2$-based photocatalysis at mesocosm scale under environmental conditions, allowing future development of *in situ* treatment for the reduction of cyanobacteria and their toxins.

## Declaration of Competing Interest

The authors declare that they have no known competing financial interests or personal relationships that could have influenced the work reported in this paper.


## Acknowledgments

The authors would like to acknowledge the Engineering and Physical Sciences Research Council (EPSRC) [EP/P029280/1], the Coordination for the

Improvement of Higher Education Personnel - CAPES [PROEX 20/2016 and Print 88887.311806/2018-00], the Brazilian National Research Council – CNPq [403116/2016-3 and 304164/2017-8] and the Ceará Research Support Foundation - FUNCAP [PNE-0112-00042.01.00/16] for funding this research.

## References

Amaral-Zettler, L.A., McCliment, E.A., Ducklow, H.W., Huse, S.M., 2009. A method for studying protistan diversity using massively parallel sequencing of V9 hypervariable regions of small-subunit ribosomal RNA Genes. PLoS One 4. https://doi.org/10.1371/journal.pone.0006372

Andrews, S., 2010. FastQC: A Quality COntrol Toll for High Throughput Sequence Data [WWW Document]. URL http://www.bioinformatics.babraham.ac.uk/projects/fastqc

Asker, D., Awad, T.S., Beppu, T., Ueda, K., 2012. Isolation, characterization, and diversity of novel radiotolerant carotenoid-producing bacteria. Methods Mol. Biol. 892, 21–60. https://doi.org/10.1007/978-1-61779-879-5_3

Båmstedt, U., Larsson, H., 2018. An indoor pelagic mesocosm facility to simulate multiple water-column characteristics. Int. Aquat. Res. 10, 13–29. https://doi.org/10.1007/s40071-017-0185-y

Barros, M.U.G., Wilson, A.E., Leitão, J.I.R., Pereira, S.P., Buley, R.P., Fernandez-Figueroa, E.G., Capelo-Neto, J., 2019. Environmental factors associated with toxic cyanobacterial blooms across 20 drinking water

855 reservoirs in a semi-arid region of Brazil. Harmful Algae 86, 128–137.
856 https://doi.org/10.1016/j.hal.2019.05.006

857 Bernroitner, M., Zamocky, M., Furtmüller, P.G., Peschek, G.A., Obinger, C.,
858 2009. Occurrence, phylogeny, structure, and function of catalases and
859 peroxidases in cyanobacteria. J. Exp. Bot. 60, 423–440.
860 https://doi.org/10.1093/jxb/ern309

861 Callahan, B., 2018. Silva taxonomic training data formatted for DADA2 (Silva
862 version 132). https://doi.org/10.5281/ZENODO.1172783

863 Callahan, B.J., McMurdie, P.J., Holmes, S.P., 2017. Exact sequence variants
864 should replace operational taxonomic units in marker-gene data analysis.
865 ISME J. 11, 2639–2643. https://doi.org/10.1038/ismej.2017.119

866 Callahan, J.B., McMurdie J, P., Rosen J, M., Han W, A., Johnson A, A.J., Holmes
867 P, S., 2016. Dada2: High resolution sample inference from Illumina
868 amplicon data. Nat. Methods 13, 1–16.

869 Camacho-Muñoz, D., Fervers, A.S., Pestana, C.J., Edwards, C., Lawton, L.A.,
870 2020. Degradation of microcystin-LR and cylindrospermopsin by
871 continuous flow UV-A photocatalysis over immobilised $TiO_2$. J. Environ.
872 Manage. 276. https://doi.org/10.1016/j.jenvman.2020.111368

873 Caporaso, J.G., Lauber, C.L., Walters, W.A., Berg-Lyons, D., Lozupone, C.A.,
874 Turnbaugh, P.J., Fierer, N., Knight, R., 2011. Global patterns of 16S rRNA
875 diversity at a depth of millions of sequences per sample. Proc. Natl. Acad.
876 Sci. U.S.A. 108, 4516–4522. https://doi.org/10.1073/PNAS.1000080107/-
877 /DCSUPPLEMENTAL/PNAS.201000080SI.PDF

878 Cavalier-Smith, T., 2018. Kingdom Chromista and its eight phyla: a new
879 synthesis emphasising periplastid protein targeting, cytoskeletal and
880 periplastid evolution, and ancient divergences. Protoplasma 255, 297–357.
881 https://doi.org/10.1007/s00709-017-1147-3

882 Chun, S.J., Cui, Y., Lee, C.S., Ra Cho, A., Baek, K., Choi, A., Ko, S.R., Lee,
883 H.G., Hwang, S., Oh, H.M., Ahn, C.Y., 2019. Characterization of distinct
884 cyanohabs-related modules in microbial recurrent association network.
885 Front. Microbiol. 10. https://doi.org/10.3389/fmicb.2019.01637

886 Clemente, A., Wilson, A., Oliveira, S., Menezes, I., Gois, A., Capelo-Neto, J.,
887 2020. The role of hydraulic conditions of coagulation and flocculation on
888 the damage of cyanobacteria. Sci. Total Environ. 740, 139737.
889 https://doi.org/10.1016/j.scitotenv.2020.139737

890 Dokulil, M.T., Teubner, K., 2000. Cyanobacterial Dominance in Lakes.
891 Hydrobiologia 438, 1–12.

892 Drábková, M., Admiraal, W., Maršálek, B., 2007. Combined exposure to
893 hydrogen peroxide and light - Selective effects on cyanobacteria, green
894 algae, and diatoms. Environ. Sci. Technol. 41, 309–314.
895 https://doi.org/10.1021/es060746i

896 Fan, F., Shi, X., Zhang, M., Liu, C., Chen, K., 2019. Comparison of algal
897 harvest and hydrogen peroxide treatment in mitigating cyanobacterial
898 blooms via an *in situ* mesocosm experiment. Sci. Total Environ. 694.
899 https://doi.org/10.1016/j.scitotenv.2019.133721

900 Fan, J., Ho, L., Hobson, P., Brookes, J., 2013. Evaluating the effectiveness of

copper sulphate, chlorine, potassium permanganate, hydrogen peroxide and ozone on cyanobacterial cell integrity. Water Res. 47, 5153–5164. https://doi.org/10.1016/j.watres.2013.05.057

Fan, J., Hobson, P., Ho, L., Daly, R., Brookes, J., 2014. The effects of various control and water treatment processes on the membrane integrity and toxin fate of cyanobacteria. J. Hazard. Mater. 264, 313–322. https://doi.org/10.1016/j.jhazmat.2013.10.059

Farkas, J., Peter, H., Ciesielski, T.M., Thomas, K. V., Sommaruga, R., Salvenmoser, W., Weyhenmeyer, G.A., Tranvik, L.J., Jenssen, B.M., 2015. Impact of $TiO_2$ nanoparticles on freshwater bacteria from three Swedish lakes. Sci. Total Environ. 535, 85–93. https://doi.org/10.1016/j.scitotenv.2015.03.043

Farrell, C.C., Osman, A.I., Doherty, R., Saad, M., Zhang, X., Murphy, A., Harrison, J., Vennard, A.S.M., Kumaravel, V., Al-Muhtaseb, A.H., Rooney, D.W., 2020. Technical challenges and opportunities in realising a circular economy for waste photovoltaic modules. Renew. Sustain. Energy Rev. 128, 109911. https://doi.org/10.1016/J.RSER.2020.109911

Graupner, N., Jensen, M., Bock, C., Marks, S., Rahmann, S., Beisser, D., Boenigk, J., 2018. Evolution of heterotrophy in chrysophytes as reflected by comparative transcriptomics. FEMS Microbiol. Ecol. 94. https://doi.org/10.1093/femsec/fiy039

Grossman, A.R., Bhaya, D., Apt, K.E., Kehoe, D.M., 1995. Light-harvesting complexes in oxygenic photosynthesis: Diversity, control, and evolution.

924 Annu. Rev. Genet. https://doi.org/10.1146/annurev.ge.29.120195.001311

925 Guedes, I.A., Rachid, C.T.C.C., Rangel, L.M., Silva, L.H.S., Bisch, P.M.,
926 Azevedo, S.M.F.O., Pacheco, A.B.F., 2018. Close link between harmful
927 cyanobacterial dominance and associated bacterioplankton in a tropical
928 eutrophic reservoir. Front. Microbiol. 9.
929 https://doi.org/10.3389/fmicb.2018.00424

930 Guillou, L., Bachar, D., Audic, S., Bass, D., Berney, C., Bittner, L., Boutte, C.,
931 Burgaud, G., De Vargas, C., Decelle, J., Del Campo, J., Dolan, J.R.,
932 Dunthorn, M., Edvardsen, B., Holzmann, M., Kooistra, W.H.C.F., Lara, E.,
933 Le Bescot, N., Logares, R., Mahé, F., Massana, R., Montresor, M., Morard,
934 R., Not, F., Pawlowski, J., Probert, I., Sauvadet, A.L., Siano, R., Stoeck,
935 T., Vaulot, D., Zimmermann, P., Christen, R., 2013. The Protist Ribosomal
936 Reference database (PR2): A catalog of unicellular eukaryote Small Sub-
937 Unit rRNA sequences with curated taxonomy. Nucleic Acids Res. 41.
938 https://doi.org/10.1093/nar/gks1160

939 Gunaratne, H.Q.N., Pestana, C.J., Skillen, N., Hui, J., Saravanan, S., Edwards,
940 C., Irvine, J.T.S., Robertson, P.K.J., Lawton, L.A., 2020. 'All in one' photo-
941 reactor pod containing $TiO_2$ coated glass beads and LEDs for continuous
942 photocatalytic destruction of cyanotoxins in water. Environ. Sci. Water
943 Res. Technol. 6, 945–950. https://doi.org/10.1039/c9ew00711c

944 Hammer, Ø., Harper, D.A.T., Ryan, P.D., 2001. Past: Paleontological statistics
945 software package for education and data analysis. Palaeontol. Electron. 4.

946 Hitzfeld, B.C., Höger, S.J., Dietrich, D.R., 2000. Cyanobacterial toxins:

947 Removal during drinking water treatment, and human risk assessment.
948 Environ. Health Perspect. https://doi.org/10.1289/ehp.00108s1113

949 Hoffmann, M.R., Martin, S.T., Choi, W., Bahnemann1', D.W., Keck, W.M.,
950 1995. Environmental Applications of Semiconductor Photocatalysis. Chem.
951 Rev 95, 69–96.

952 Huang, C., Yunmei, L., Liu, G., Guo, Y., Yang, H., Zhu, A.X., Song, T., Huang,
953 T., Zhang, M., Shi, K., 2017. Tracing high time-resolution fluctuations in
954 dissolved organic carbon using satellite and buoy observations: Case study
955 in Lake Taihu, China. Int. J. Appl. Earth Obs. Geoinf. 62, 174–182.
956 https://doi.org/10.1016/J.JAG.2017.06.009

957 Huang, W.J., Lin, T.P., Chen, J.S., Shih, F.H., 2011. Photocatalytic inactivation
958 of cyanobacteria with ZnO/γ-Al2$O_3$composite under solar light. J. Environ.
959 Biol. 32, 301–307.

960 INMET - National Institute of Meteorology (Brazil), 2019. Weather Data [WWW
961 Document]. URL
962 http://www.inmet.gov.br/portal/index.php?r=bdmep/bdmep

963 Lawton, L.A., Robertson, P.K.J., Cornish, B.J.P.A., Jaspars, M., 1999.
964 Detoxification of microcystins (cyanobacterial hepatotoxins) using $TiO_2$
965 photocatalytic oxidation. Environ. Sci. Technol. 33, 771–775.
966 https://doi.org/10.1021/es9806682

967 Lawton, L.A., Robertson, P.K.J., Cornish, B.J.P.A., Marr, I.L., Jaspars, M.,
968 2003. Processes influencing surface interaction and photocatalytic
969 destruction of microcystins on titanium dioxide photocatalysts. J. Catal.

213, 109–113. https://doi.org/10.1016/S0021-9517(02)00049-0

Li, Y., Lv, K., Ho, W., Dong, F., Wu, X., Xia, Y., 2017. Hybridization of rutile $TiO_2$ ($rTiO_2$) with g-$C_3N_4$ quantum dots (CN QDs): An efficient visible-light-driven Z-scheme hybridized photocatalyst. Appl. Catal. B Environ. 202, 611–619. https://doi.org/10.1016/j.apcatb.2016.09.055

Litchman, E., Edwards, K.F., Klausmeier, C.A., 2015. Microbial resource utilization traits and trade-offs: Implications for community structure, functioning, and biogeochemical impacts at present and in the future. Front. Microbiol. 6. https://doi.org/10.3389/fmicb.2015.00254

Liu, I., Lawton, L.A., Robertson, P.K.J., 2003. Mechanistic studies of the photocatalytic oxidation of microcystin-LR: An investigation of byproducts of the decomposition process. Environ. Sci. Technol. 37, 3214–3219. https://doi.org/10.1021/es0201855

Liu, L., Chen, H., Liu, M., Yang, J.R., Xiao, P., Wilkinson, D.M., Yang, J., 2019. Response of the eukaryotic plankton community to the cyanobacterial biomass cycle over 6 years in two subtropical reservoirs. ISME J. 13, 2196–2208. https://doi.org/10.1038/s41396-019-0417-9

Loeb, S.K., Alvarez, P.J.J., Brame, J.A., Cates, E.L., Choi, W., Crittenden, J., Dionysiou, D.D., Li, Q., Li-Puma, G., Quan, X., Sedlak, D.L., David Waite, T., Westerhoff, P., Kim, J.-H., Byers, B., 2019. The Technology Horizon for Photocatalytic Water Treatment: Sunrise or Sunset? Environ. Sci. Technol 53, 45. https://doi.org/10.1021/acs.est.8b05041

Marques, É.T., Gunkel, G., Sobral, M.C., 2019. Management of tropical river

basins and reservoirs under water stress: Experiences from northeast Brazil. Environ. - MDPI 6. https://doi.org/10.3390/environments6060062

Martin, M., 2011. Cutadapt removes adapter sequences from high-throughput sequencing reads. EMBnet.journal. https://doi.org/10.14806/ej.17.1.200

Martínez-Laborda, A., Balsalobre, J.M., Fontes, M., Murillo, F.J., 1990. Accumulation of carotenoids in structural and regulatory mutants of the Bacterium *Myxococcus xanthus*. MGG Mol. Gen. Genet. 223, 205–210. https://doi.org/10.1007/BF00265055

Menezes, I., Capelo-Neto, J., Pestana, C.J., Clemente, A., Hui, J., Irvine, J.T.S., Nimal Gunaratne, H.Q., Robertson, P.K.J., Edwards, C., Gillanders, R.N., Turnbull, G.A., Lawton, L.A., 2021. Comparison of UV-A photolytic and UV/$TiO_2$ photocatalytic effects on *Microcystis aeruginosa* PCC7813 and four microcystin analogues: A pilot scale study. J. Environ. Manage. 298, 113519. https://doi.org/10.1016/j.jenvman.2021.113519

Méresse, S., Fodil, M., Fleury, F., Chénais, B., 2020. Fucoxanthin, a marine-derived carotenoid from brown seaweeds and microalgae: A promising bioactive compound for cancer therapy. Int. J. Mol. Sci. https://doi.org/10.3390/ijms21239273

Nicholls, K.H., Wujek, D.E., 2003. Chrysophycean Algae, in: Wehr, J., Sheath, R., Kociolek, J.P. (Eds.), Freshwater Algae of North America: Ecology and Classification. Elsevier Inc. Academic Press, San Diego, CA, USA, pp. 471–509. https://doi.org/10.1016/B978-012741550-5/50013-1

Paerl, H.W., Huisman, J., 2008. Climate: Blooms like it hot. Science (80-. ).

320, 57–58. https://doi.org/10.1126/science.1155398

Passardi, F., Zamocky, M., Favet, J., Jakopitsch, C., Penel, C., Obinger, C., Dunand, C., 2007. Phylogenetic distribution of catalase-peroxidases: Are there patches of order in chaos? Gene 397, 101–113. https://doi.org/10.1016/j.gene.2007.04.016

Pestana, C.J., Capelo-Neto, J., Lawton, L., Oliveira, S., Carloto, I., Linhares, H.P., 2019. The effect of water treatment unit processes on cyanobacterial trichome integrity. Sci. Total Environ. 659, 1403–1414. https://doi.org/10.1016/j.scitotenv.2018.12.337

Pestana, C.J., Hobson, P., Robertson, P.K.J., Lawton, L.A., Newcombe, G., 2020a. Removal of microcystins from a waste stabilisation lagoon: Evaluation of a packed-bed continuous flow $TiO_2$ reactor. Chemosphere 245, 125575. https://doi.org/10.1016/j.chemosphere.2019.125575

Pestana, C.J., Lawton, L.A., Kaloudis, Triantafyllos, 2020b. Removal and/or Destruction of Taste and Odour Compound by Conventional and Advanced Oxidation Processes, in: Hiskia, A.E., Triantis, T.M., Antoniou, M.G., Kaloudis, T., Dionysiou, D.D. (Eds.), Water Treatment for Purification from Cyanobacteria and Cyanotoxins. John Wiley & Sons Ltd, Hoboken, NJ, pp. 207–230.

Pestana, C.J., Portela Noronha, J., Hui, J., Edwards, C., Gunaratne, H.Q.N., Irvine, J.T.S., Robertson, P.K.J., Capelo-Neto, J., Lawton, L.A., 2020c. Photocatalytic removal of the cyanobacterium *Microcystis aeruginosa* PCC7813 and four microcystins by $TiO_2$ coated porous glass beads with

UV-LED irradiation. Sci. Total Environ. 745, 141154. https://doi.org/10.1016/j.scitotenv.2020.141154

Pestana, C.J., Robertson, P.K.J., Edwards, C., Wilhelm, W., McKenzie, C., Lawton, L.A., 2014. A continuous flow packed bed photocatalytic reactor for the destruction of 2-methylisoborneol and geosmin utilising pelletised $TiO_2$. Chem. Eng. J. 235, 293–298. https://doi.org/10.1016/j.cej.2013.09.041

R Core Team, 2020. R: A language and environment for statistical computing [WWW Document]. R Found. Stat. Comput. Vienna, Austria. URL https://www.r-project.org/

Robertson, P.K.J., Lawton, L. A., Cornish, B.J.P.A., Jaspars, M., 1998. Processes influencing the destruction of microcystin-LR by $TiO_2$ photocatalysis. J. Photochem. Photobiol. A Chem. 116, 215–219. https://doi.org/10.1016/S1010-6030(98)00312-8

Robertson, P.K.J., Lawton, L.A., Cornish, B.J.P.A., 1998. The Involvement of Phycocyanin Pigment in the Photodecomposition of the Cyanobacterial Toxin, Microcystin-LR. J. Porphyr. Phthalocyanines 3, 554–551. https://doi.org/https://doi.org/10.1002/(SICI)1099-1409(199908/10)3:6/7<544::AID-JPP173>3.0.CO;2-7

Robertson, P.K.J., Lawton, L.A., Münch, B., Rouzade, J., 1997. Destruction of cyanobacterial toxins by semiconductor photocatalysis. Chem. Commun. 393–394. https://doi.org/10.1039/a607965b

Rognes, T., Flouri, T., Nichols, B., Quince, C., Mahé, F., 2016. VSEARCH: A

versatile open source tool for metagenomics. PeerJ 2016. https://doi.org/10.7717/peerj.2584

Santos, A.A., Guedes, D.O., Barros, M.U.G., Oliveira, S., Pacheco, A.B.F., Azevedo, S.M.F.O., Magalhães, V.F., Pestana, C.J., Edwards, C., Lawton, L.A., Capelo-Neto, J., 2021. Effect of hydrogen peroxide on natural phytoplankton and bacterioplankton in a drinking water reservoir: Mesocosm-scale study. Water Res. 197, 117069. https://doi.org/10.1016/j.watres.2021.117069

Simpson, A.G.B., Eglit, Y., 2016. Protist diversification, in: Kliman, R.M. (Ed.), Encyclopedia of Evolutionary Biology Volume 3. Elsevier, Amsterdam, pp. 344–360.

Slade, D., Radman, M., 2011. Oxidative Stress Resistance in *Deinococcus radiodurans*. Microbiol. Mol. Biol. Rev. 75, 133–191. https://doi.org/10.1128/mmbr.00015-10

Stafsnes, M.H., Josefsen, K.D., Kildahl-Andersen, G., Valla, S., Ellingsen, T.E., Bruheim, P., 2010. Isolation and characterization of marine pigmented bacteria from Norwegian coastal waters and screening for carotenoids with UVA-blue light absorbing properties. J. Microbiol. 48, 16–23. https://doi.org/10.1007/s12275-009-0118-6

Sun, L., Wang, L., Li, J., Liu, H., 2014. Characterization and antioxidant activities of degraded polysaccharides from two marine Chrysophyta. Food Chem. 160, 1–7. https://doi.org/10.1016/j.foodchem.2014.03.067

Takebe, F., Hara, I., Matsuyama, H., Yumoto, I., 2007. Effects of H2O2 under

Low- and High-Aeration-Level Conditions on Growth and Catalase Activity in *Exiguobacterium oxidotolerans* T-2-2T. J. Biosci. Bioeng. 104, 464–469. https://doi.org/10.1263/jbb.104.464

Tõnno, I., Agasild, H., Kõiv, T., Freiberg, R., Nõges, P., Nõges, T., 2016. Algal diet of small-bodied crustacean zooplankton in a cyanobacteria-dominated eutrophic lake. PLoS One 11, e0154526. https://doi.org/10.1371/journal.pone.0154526

Tytler, E.M., Wong, T., Codd, G.A., 1984. Photoinactivation in vivo of superoxide dismutase and catalase in the cyanobacterium *Microcystis aeruginosa*. FEMS Microbiol. Lett. 23, 239–242. https://doi.org/10.1111/j.1574-6968.1984.tb01070.x

Vaissie, P., Monge, A., Hudsson, F., 2020. Fac toshiny: Perform Factorial Analysis from "FactoMineR" with a Shiny Application. R-package version 2.2.

Winnepenninckx, B., Backeljau, T., De Wachter, R., 1993. Extraction of high molecular weight DNA from molluscs. Trends Genet. 9, 407. https://doi.org/10.1016/0168-9525(93)90102-n

Yang, Z., Buley, R.P., Fernandez-Figueroa, E.G., Barros, M.U.G., Rajendran, S., Wilson, A.E., 2018. Hydrogen peroxide treatment promotes chlorophytes over toxic cyanobacteria in a hyper-eutrophic aquaculture pond. Environ. Pollut. 240, 590–598. https://doi.org/10.1016/j.envpol.2018.05.012

Ye, L., Wu, X., Liu, B., Yan, D., Kong, F., 2015. Dynamics and sources of dissolved organic carbon during phytoplankton bloom in hypereutrophic

Lake Taihu (China). Limnologica 54, 5–13. https://doi.org/10.1016/J.LIMNO.2015.05.003

Yilmaz, P., Parfrey, L.W., Yarza, P., Gerken, J., Pruesse, E., Quast, C., Schweer, T., Peplies, J., Ludwig, W., Glöckner, F.O., 2014. The SILVA and "all-species Living Tree Project (LTP)" taxonomic frameworks. Nucleic Acids Res. 42. https://doi.org/10.1093/nar/gkt1209

Zamyadi, A., Macleod, S.L., Fan, Y., Mcquaid, N., Dorner, S., Sauvé, S., Prévost, M., 2012. Toxic cyanobacterial breakthrough and accumulation in a drinking water plant: A monitoring and treatment challenge. Water Res. 46, 1511–1523. https://doi.org/10.1016/j.watres.2011.11.012

Zhang, L., Lyu, K., Wang, N., Gu, L., Sun, Y., Zhu, X., Wang, J., Huang, Y., Yang, Z., 2018. Transcriptomic Analysis Reveals the Pathways Associated with Resisting and Degrading Microcystin in Ochromonas. Environ. Sci. Technol. 52, 11102–11113. https://doi.org/10.1021/acs.est.8b03106

Zhang, L., Yang, J., Liu, L., Wang, N., Sun, Y., Huang, Y., Yang, Z., 2021. Simultaneous removal of colonial *Microcystis* and microcystins by protozoa grazing coupled with ultrasound treatment. J. Hazard. Mater. 420. https://doi.org/10.1016/j.jhazmat.2021.126616

Zheng, Q., Wang, Y., Lu, J., Lin, W., Chen, F., Jiao, N., 2020. Metagenomic and metaproteomic insights into photoautotrophic and heterotrophic interactions in a *Synechococcus* culture. MBio 11. https://doi.org/10.1128/mBio.03261-19

# Supplementary Information for:

## Selective suppression of cyanobacteria using $TiO_2$-based photocatalysis *in situ*: short term evaluation in a drinking water reservoir

Carlos J. Pestana[a*†], Allan Amorim Santos[b*], Samylla Oliveira[c], Ricardo Rogers[b], Jianing Hui[d], Nathan C. Skillen[e], Christine Edwards[a], José Capelo-Neto[c], Sandra M.F.O. Azevedo[b], Peter K.J. Robertson[e], John T.S. Irvine[d], Linda A. Lawton[a]

* These two authors have contributed equally to the manuscript

† corresponding author: c.pestana@rgu.ac.uk

[a] School of Pharmacy and Life Sciences, Robert Gordon University, Aberdeen, UK

[b] Institute of Biophysics Carlos Chagas Filho, Federal University of Rio de Janeiro, Rio de Janeiro, Brazil

[c] Department of Hydraulic and Environmental Engineering, Federal University of Ceará, Fortaleza, Brazil

[d] School of Chemistry, University of St. Andrews, St. Andrews, UK

[e] School of Chemistry and Chemical Engineering, Queen's University Belfast, Belfast, UK

# S1 Meteorological Data

**Table S1:** Meteorological condition observed between October and November 2019 at Fortaleza city according to the National Institute of Meteorology – INMET. The data are expressed as averages from daily measurements.

| Avg. Temp. (ºC) | Humidity (%) | Atmospheric pressure (hPa) | Wind velocity (m/s) | Solar irradiance (h) | Max. Temp. (ºC) | Min. Temp. (ºC) | Precipitation (mm) |
|---|---|---|---|---|---|---|---|
| 27.7 ± 1.2 | 74 ± 8.7 | 1009.6 ± 1.2 | 3.01 ± 1.0 | 10.2 ± 0.7 | 32.2 ± 0.5 | 25.0 ± 0.6 | 0.05 ± 0.2 |

# S2 Materials and Methods

## S2.1 Physicochemical analyses

**Table S2:** Physical and chemical parameters measured *in situ* or in the laboratory (all methods apart from transparency determination according to APHA, 2012).

| Parameter (unit) | Equipment/Method | Where |
|---|---|---|
| Transparency (cm) | Secchi disk | *in situ* |
| Temperature (°C) and pH | YSI probe model 55 and 60 (Yellow Springs Instruments, EUA) / APHA 4500 H-B | *in situ* |
| Dissolved oxygen (mg/L) | YSI probe model 55 (Yellow Springs Instruments, EUA) / APHA 4500 O-G | *in situ* |
| Conductivity (µS/cm) | Conductivity meter 105A+ (Orion Research, EUA) / APHA2510-A | *in situ* |
| Turbidity (NTU) | Hach model 2100P (EUA) / APHA2130-B | Laboratory |
| True color (uC) | Genesys spectrophotometer 10S UV-Vis – (Thermo Scientific, EUA) / APHA2120-C | Laboratory |
| Total organic carbon (TOC) and dissolved carbon (DOC) (mg $L^{-1}$) | Sievers InnovOx Laboratory TOC Analyzer (General Electrics, USA) / APHA5310 | Laboratory |

| | | |
|---|---|---|
| Nitrite, nitrate, orthophosphate, sulfate, fluoride, and chloride (mg $L^{-1}$). | Samples were filtered through a glass fiber 0.45-µm membrane before analyses by Ion Chromatograph using Dionex ICS-1100 (Thermo Scientific, EUA) / APHA4110-C | Laboratory |

## S2.2 Statistical analysis

### S2.2.1 Abiotic factors

Principal component analysis (PCA) was performed as a nonlinear multivariate statistical technique, used to determine the relationships between the physical and chemical environmental parameters analyzed from the control and treatment samples over time. PCA was also used to gather the data in groups according to their variances in the different dimensional axes (Savegnago et al., 2011). A selection of the parameters for PCA ordination was conducted following their importance related to the effect of the treatment as well as the size of the vector (considering $cos^2$ value) and the contribution with at least more than 70% of dimensionality variance from the principal components. Subsequently, clustering was carried out using the Canberra distance (Riba et al., 2020) and Ward's method.

For each physical and chemical parameter considered relevant from PCA and non-normal distribution (following Shapiro-Wilk $p<0.05$), a Wilcoxon-Mann-Whitney test was performed to show significant differences ($p<0.05$) between the two groups and identify, one by one, the parameters that could show the efficiency of the photocatalytic treatment with $TiO_2$. Statistical analyzes were performed using R software version 3.4.1, using the Factoshiny package (Vaissie et al., 2020).

### S2.2.2 Biotic factors (bacterial and eukaryotic plankton communities)

Alpha-diversity estimators were calculated and tested for normality considering the Shapiro-Wilk test, skewness, and kurtosis, to evaluate significant differences between treatment and control at each sampling time. As Shannon diversity and estimated richness (observed species) from 16S rRNA data were parametric, a two-way analysis of variance test was used for multiple comparisons of means at a 95% confidence interval considering time and condition (treatment and control) as factors, whereas for 18S rRNA data, we used the Kruskal-Wallis non-parametric test.

From the 18S rRNA data, we used the taxonomic groups identified and gathered the main taxa (>3% relative abundance in at least one sample) in relevant freshwater plankton groups, following the classification described in previous studies (Cavalier-Smith, 2018; Simpson and Eglit, 2016) (Table S2).

The beta-diversity ordination was evaluated by nMDS (non-metric dimensional scaling) considering ASVs abundance in a tridimensional space using the Bray-Curtis distance as dissimilarity matrix. Then, it was complemented by permutational multivariate analysis of variance (two-way PERMANOVA, $p<0.05$) using two factors as experimental condition (control or $TiO_2$) and time (0, 3 and 7). In the null-hypothesis, $TiO_2$ did not affect the bacterial and eukaryotic plankton communities; alternatively, we assumed that the treatment modified the structure of both communities.

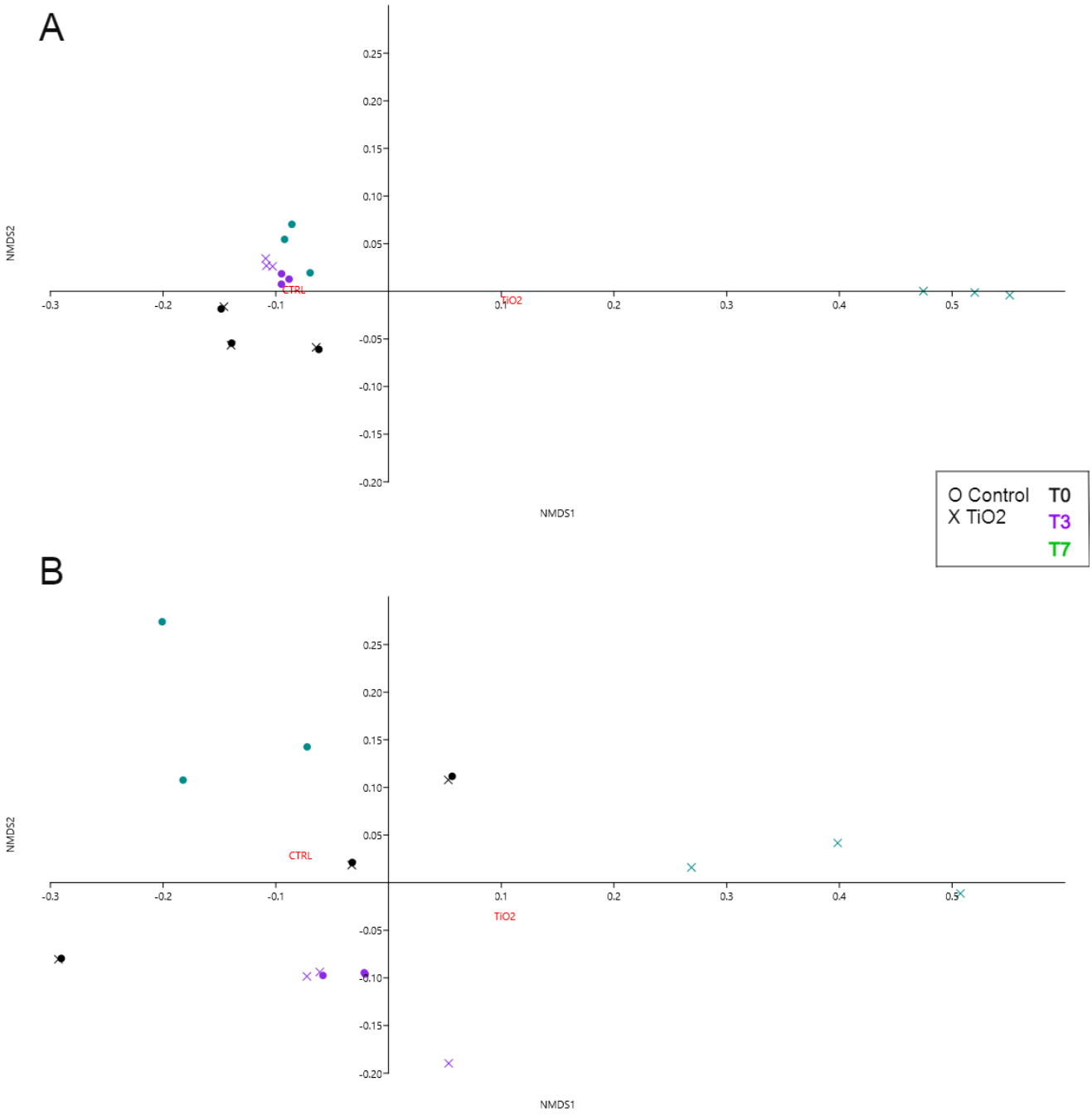


Figure S1: Beta diversity considering samples ordination according to the Bacteria (A) and Eukarya (B) composition by non-metric multidimensional scaling (nMDS) using Bray-Curtis distance. Samples correspond to control (circle) or $TiO_2$/UV treatment (X) collected over the time 0, 3 and 7 days (n=3).

**Table S3:** Internal assignment of most representative 18S taxa considering relevant groups of freshwater biotic system following taxonomic classification of Cavalier-Smith (2018) and Simpson and Eglit (2016).

| Defined Groups | Representative Taxa | Kingdom | Phylum | Observed Genus |
|---|---|---|---|---|
| Chlorophyte | *Chlorophyta* | Plantae | *Chlorophyta* | Unclassified |
| Diatom | *Bacillariophyceae* | Chromista | *Bacillariophyta* | Nitzschia / Navicula / Unclassified |
| | *Fragilariales* | | *Bacillariophyta* | Ulnaria / Unclassified |
| | *Mediophyceae* | | *Bacillariophyta* | Cyclotella / Unclassified |
| Chrysophyte | *Chrysophyceae* | | *Ochrophyta* | Unclassified |
| | *Chromulinales* | | *Ochrophyta* | Poteriospumella / Poterioochromonas / Oikomonas / Unclassified |
| | *Ochromonadales* | | *Ochrophyta* | Paraphysomonas / Ochromonas / Unclassified |
| Cryptophyte | *Cryptophyceae* | | *Cryptophyta* | Unclassified |
| Alveolata | *Dinoflagellata* | | *Miozoa* | Unclassified |
| | *Perkinsidae* | | *Miozoa* | Unclassified |
| Alveolata | *Colpodellida* | | *Miozoa* | Colpodella |
| | *Choreotrichia* | | *Ciliophora* | Tintinnidium / Unclassified |
| | *Hypotrichia* | | *Ciliophora* | Halteria / Oxytricha / Stylonychia / Pseudourostyla / Unclassified |
| Discicristata/ Euglenid | *Neobodonida* | Protozoa | *Euglenozoa* | Rhynchobodo / Neobodo / Rhynchomonas / Unclassified |
| | *Prokinetoplastina* | | *Euglenozoa* | Ichthyobodo |
| | *Discicristata* | | *Uncertain* | Unclassified |
| Nucleariids | *Nucleariidae* | | *Choanozoa* | Unclassified |
| Zooplakton | *Gastrotricha* | Animalia | *Gastrotricha* | Nuclearia / Unclassified |
| | *Copepoda* | | *Arthropoda* | Calanoida / Cyclopoida / Unclassified |
| | *Podocopa* | | *Arthropoda* | Unclassified |
| | *Monogononta* | | *Rotifera* | Ploimida / Floscularia / Unclassified |
| Fungi | *Blastocladiales* | Fungi | *Blastocladiomycota* | Catenaria |
| Eukaryotic picoplankton | *Eukaryotic_ picoplankton_ environmental_ sample* | Uncertain | *Uncertain* | Unclassified |
| Unclassified | *MAST_12C* | | *Uncertain* | Unclassified |
| | *Incertae_division* | | *Uncertain* | Unclassified |
| Eukarya_uncl | *Eukarya_uncl* | | *Uncertain* | Unclassified |
| Stramenopiles_ uncl | *Stramenopiles_ uncl* | Chromista | *Stramenopiles* | Unclassified |

We also performed a linear discriminant analysis (LDA) and effect Size (LEfSe) (Segata et al., 2011) following the Hutlab Galaxy web framework (http://huttenhower.sph.harvard.edu/galaxy/) using 3.5 as LDA threshold (log 10 transformed) to select microbial taxa with a significant contribution ($p<0.05$) to the differentiation between treatment and control. For that, we applied a two-tailed non-parametric Kruskal-Wallis test and unpaired Wilcoxon test to reveal significant differences in most abundant ASVs.

**S2.3 Correlation between biotic and abiotic factors**

To test the correlation between abiotic and biotic (ASVs) factors and differences in the community structure over time, the samples were ordained by Canonical Correspondence Analysis (CCA) using the Hellinger-transformed abundance matrix and Spearman analysis ($p<0.05$ and a threshold for r value $=\pm0.4$). The analyses were performed, and charts plotted in R v3.5.3 environment (R Core Team, 2016) and Past3 software (Hammer et al., 2001).

## S3 Effect of $TiO_2$-photocatalysis on bacterioplankton

**Table S4:** Relative abundance of bacterioplankton at phylum level, considering mean and standard deviation (n=3) expressed as percentage (%) of total bacterioplankton. * Taxa classified as 'Others' in the abundance chart.

| Phylum | T0 | Day 3 | | Day 7 | |
|---|---|---|---|---|---|
| | | Control | $TiO_2$ | Control | $TiO_2$ |
| *Acidobacteria** | 0.1±0.02 | 0.1±0.003 | 0.2±0.05 | 0.05±0.02 | 0.6±0.2 |
| *Actinobacteria* | 0.9±0.32 | 3.8±0.48 | 4.4±0.22 | 5.4±0.45 | 4±0.75 |
| *Armatimonadetes** | 0.4±0.33 | 0.5±0.7 | 0.2±0.04 | 0.2±0.12 | 6.8±1.56 |
| *Bacteroidetes* | 13.6±3.2 | 14.9±1.6 | 14±1.23 | 10.7±2.9 | 35±4.94 |
| *Chlamydiae** | 0.01±0.003 | 0.08±0.01 | 0.07±0.02 | 0.6±0.3 | 0.06±0.03 |
| *Chloroflexi** | 1.9±0.9 | 2.4±0.4 | 2.3±0.6 | 3.8±1.4 | 0.6±0.2 |
| *Cyanobacteria* | 44±10.4 | 32.8±0.9 | 34±2.6 | 24.2±5.2 | 4.4±1.9 |
| *Dependentiae** | 0.03±0.02 | 0.1±0.07 | 0.1±0.02 | 0.04±0.01 | 0.07±0.02 |
| *Firmicutes** | 0.18±0.06 | 0.07±0.02 | 0.1±0.01 | 0.06±0.05 | 0.03±0.01 |
| *Gemmatimonadetes** | 0.07±0.004 | 0.3±0.05 | 0.36±0.09 | 0.14±0.03 | 1.3±0.63 |
| *Hydrogenedentes** | 0.09±0.06 | 0.04±0.02 | 0.04±0.02 | 0.01±0.007 | 0.01±0.002 |
| *Omnitrophicaeota** | 0.01±0.01 | 0.06±0.04 | 0.06±0.02 | 0.01±0.002 | 0.01±0.01 |
| *Planctomycetes* | 13.9±2.42 | 14.3±1.58 | 13.2±2.03 | 18.6±2.23 | 5.7±1.97 |
| *Proteobacteria* | 11.4±0.92 | 11.8±0.78 | 13.3±1.13 | 12.4±2.62 | 23.8±4.56 |
| *Spirochaetes** | 0.01±0.007 | 0.15±0.06 | 0.15±0.05 | 0.15±0.01 | 0.17±0.01 |
| *Verrucomicrobia* | 13.5±7.9 | 18.4±0.9 | 17.6±0.9 | 23.6±0.7 | 17.3±3.3 |

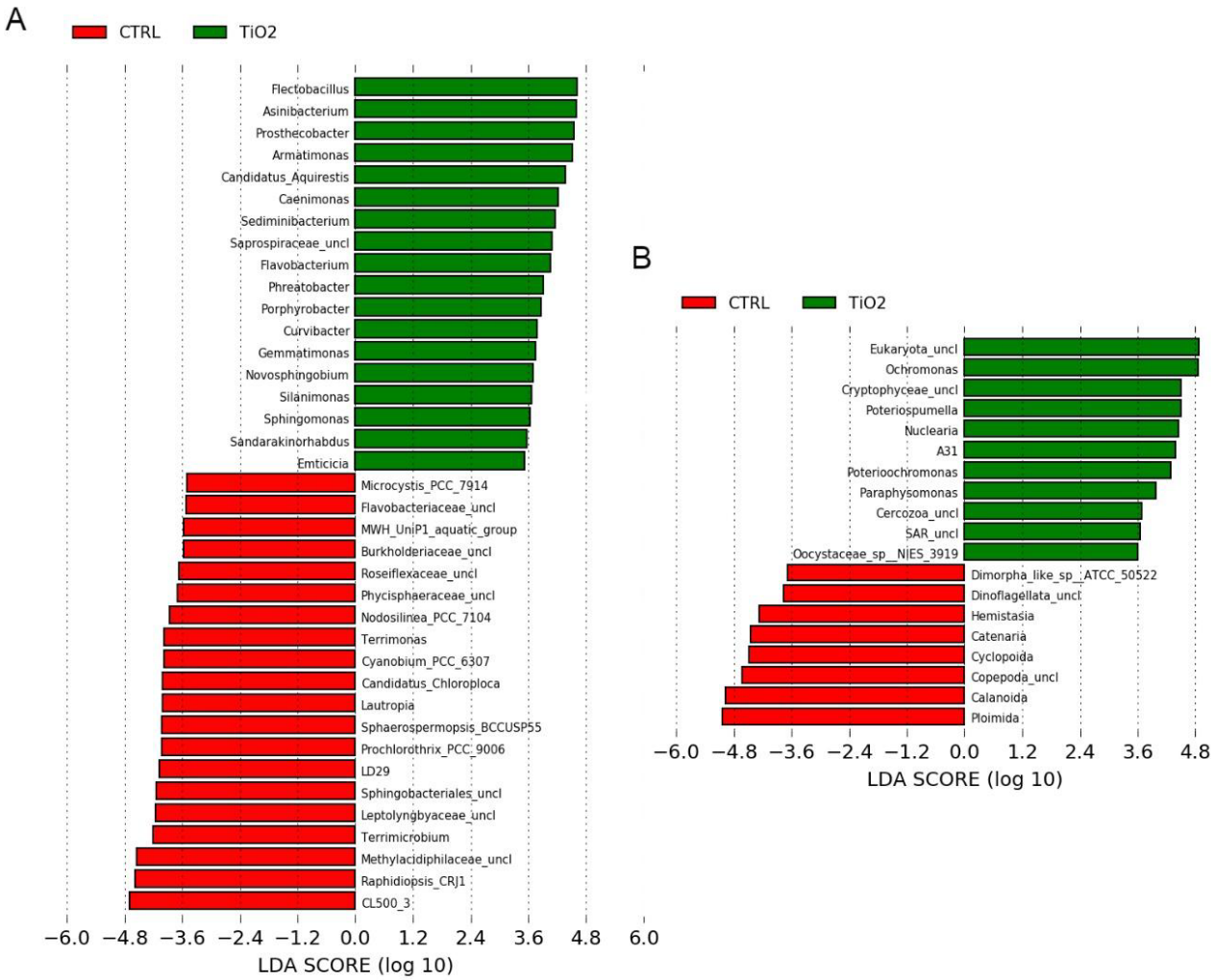


**Figure S2:** Linear discriminant analysis coupled to effect size (LEfSe) of bacterial (A) and eukaryotic (B) plankton communities considering abundance of the main taxa in treatment and control at day 7. Taxa with significantly different distribution between treatment ($TiO_2$) and control groups were selected using a p-value < 0.05 and a LDA score (log10) > 3.5.

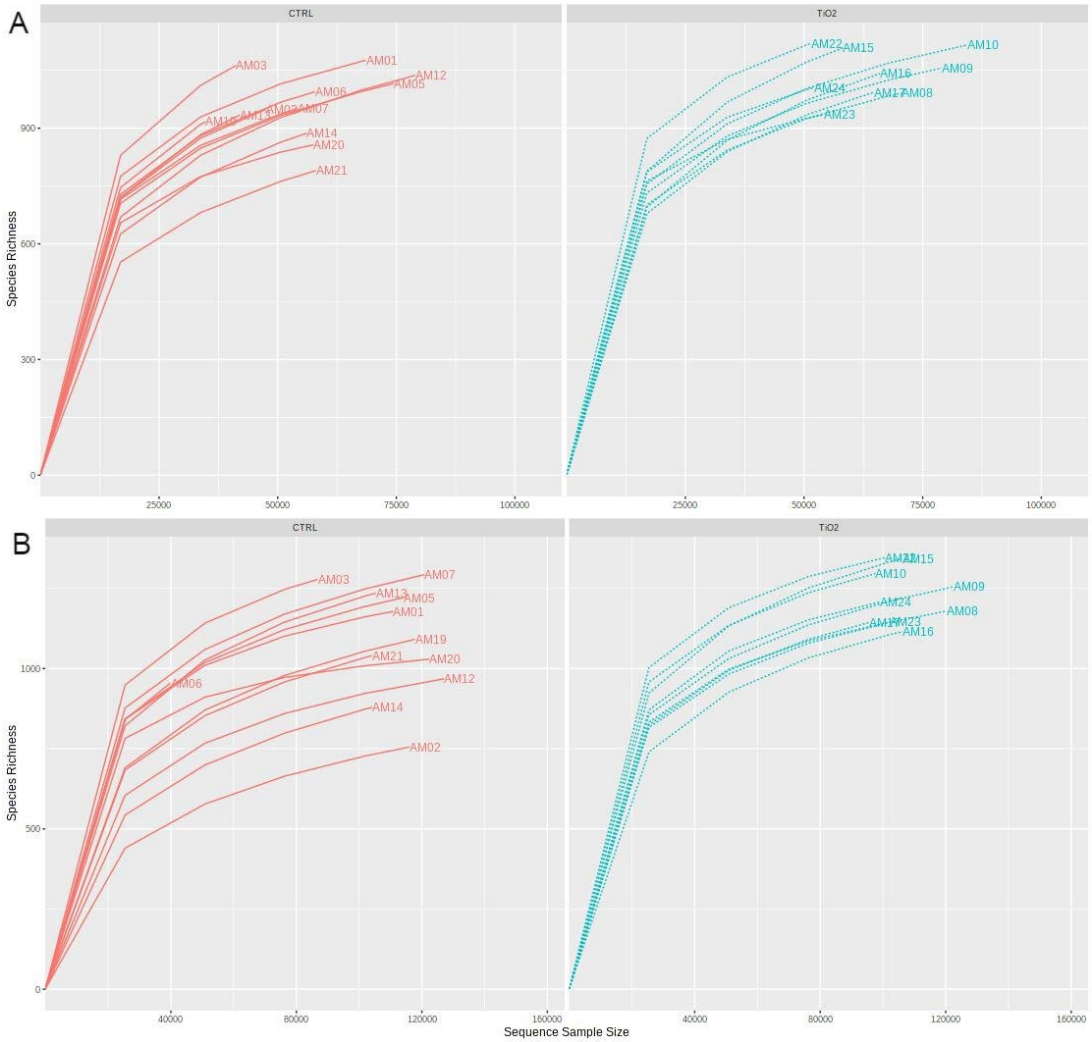


**Figure S3:** Rarefaction curve of samples from 16 rRNA (A) and 18S rRNA (B) amplicon sequencing indicating the sequencing coverage estimated from the number of species (ASVs). Samples from $TiO_2$-treatment (green) or control (red).

**Table S5:** Sample identification, sequencing data and diversity indices for 16S and 18S information. The red line for the AM06 sample (from 18S) means this sample was considered an outlier due the very low sequences number compared to others.

| Sample | Description | DNA concentration (ng $\mu L^{-1}$) | Number of sequences | | Goods | Richness | Diversity |
|---|---|---|---|---|---|---|---|
| | | | Before trim qual | After trim qual | | Sobs | Shannon (H') |
| **16S sequencing information** | | | | | | | |
| AM01 | T0 | 365.2 | 68595 | 34791 | 99.69386 | 1096 | 4.688125 |
| AM02 | T0 | 380.35 | 47565 | 34791 | 99.51014 | 978 | 4.839721 |
| AM03 | T0 | 329.64 | 41260 | 34791 | 99.35046 | 1074 | 4.770999 |
| AM05 | No $TiO_2$ (T3) | 183.98 | 74505 | 34791 | 99.71009 | 1016 | 4.857933 |
| AM06 | No $TiO_2$ (T3) | 158.19 | 57948 | 34791 | 99.62898 | 1008 | 4.836678 |
| AM07 | No $TiO_2$ (T3) | 420.96 | 54241 | 34791 | 99.60178 | 966 | 4.827779 |
| AM08 | $TiO_2$ (T3) | 290.99 | 70512 | 34791 | 99.70218 | 1008 | 4.787438 |
| AM09 | $TiO_2$ (T3) | 199.59 | 79037 | 34791 | 99.71785 | 1083 | 4.773695 |
| AM10 | $TiO_2$ (T3) | 223.54 | 84463 | 34791 | 99.73716 | 1131 | 4.909822 |
| AM12 | No $TiO_2$ (T7) | 550.73 | 79012 | 34791 | 99.65955 | 1060 | 4.675476 |
| AM13 | No $TiO_2$ (T7) | 210.94 | 41995 | 34791 | 99.41183 | 951 | 4.695779 |
| AM14 | No $TiO_2$ (T7) | 202.42 | 56182 | 34791 | 99.57104 | 909 | 4.665011 |
| AM15 | $TiO_2$ (T7) | 206.89 | 58239 | 34791 | 99.51407 | 1137 | 4.758776 |
| AM16 | $TiO_2$ (T7) | 180.4 | 66043 | 34791 | 99.57906 | 1062 | 4.489167 |
| AM17 | $TiO_2$ (T7) | 339.97 | 64669 | 34791 | 99.60723 | 1015 | 4.470062 |
| | **18S sequencing information** | | | | | | |
| AM01 | T0 | 365.2 | 110933 | 87335 | 99.82242 | 1195 | 4.130155 |
| AM02 | T0 | 380.35 | 116267 | 87335 | 99.8168 | 760 | 1.522841 |
| AM03 | T0 | 329.64 | 87335 | 87335 | 99.72978 | 1311 | 4.647847 |
| AM05 | No $TiO_2$ (T3) | 183.98 | 114505 | 87335 | 99.78604 | 1225 | 4.193731 |
| AM06 | No $TiO_2$ (T3) | 158.19 | 39861 | xx | 99.35024 | 955 | 3.943944 |
| AM07 | No $TiO_2$ (T3) | 420.96 | 120900 | 87335 | 99.78577 | 1296 | 4.562986 |
| AM08 | $TiO_2$ (T3) | 290.99 | 120383 | 87335 | 99.83054 | 1181 | 3.872202 |
| AM09 | $TiO_2$ (T3) | 199.59 | 122645 | 87335 | 99.80431 | 1260 | 4.143498 |
| AM10 | $TiO_2$ (T3) | 223.54 | 97579 | 87335 | 99.752 | 1303 | 5.213536 |
| AM12 | No $TiO_2$ (T7) | 550.73 | 127122 | 87335 | 99.83952 | 972 | 3.066831 |

| | | | | | | | |
|---|---|---|---|---|---|---|---|
| AM13 | No $TiO_2$ (T7) | 210.94 | 105336 | 87335 | 99.73798 | 1243 | 3.883575 |
| AM14 | No $TiO_2$ (T7) | 202.42 | 104105 | 87335 | 99.74641 | 881 | 3.2469 |
| AM15 | $TiO_2$ (T7) | 206.89 | 106102 | 87335 | 99.73987 | 1354 | 4.44185 |
| AM16 | $TiO_2$ (T7) | 180.4 | 106361 | 87335 | 99.77811 | 1123 | 3.389061 |
| AM17 | $TiO_2$ (T7) | 339.97 | 95848 | 87335 | 99.75795 | 1153 | 4.165068 |

159

160

161

162

163

164

165

166

167

168

169

170

171

172

173

174

175

176

177

178

## S4 Effect $TiO_2$-photocatalysis on abiotic factors (water quality)

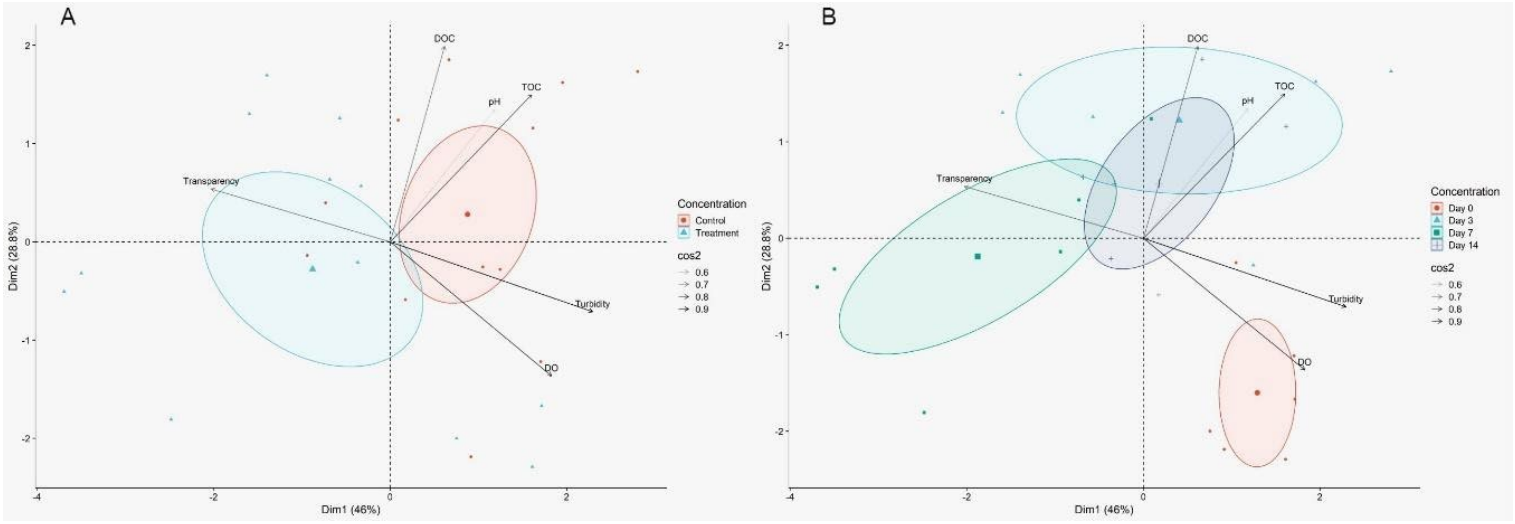


**Figure S4:** Ordination of the most relevant abiotic parameters considering treatment (A) and time (B) following Principal Component Analysis (PCA) and Ward distance. Both dimensions contributed to explain about 75% of variance of data and the correlation among the parameters.

**Table S6:** Effect of TiO2-photocatalysis on dissolved nutrient, sulfate, fluoride and chloride content in water. Data are expressed as average and standard deviation (n=3).

| | Raw water (T0) | Day 3 | | Day 7 | |
|---|---|---|---|---|---|
| | | $TiO_2$ | Control | $TiO_2$ | Control |
| **Nitrite (mg $L^{-1}$)** | 0.77 ± 0.03 | 0.76 ± 0.01 | 0.77 ± 0.03 | 0.77 ± 0.02 | 0.78 ± 0.02 |
| **Nitrate (mg $L^{-1}$)** | 0.82 ± 0.27 | 0.42 ± 0.05 | 0.71 ± 0.04 | 0.61 ± 0.12 | 0.62 ± 0.04 |
| **Orthophosphate (mg $L^{-1}$)** | 0.55 ± 0.1 | 0.93 ± 0.18 | 0.80 ± 0.12 | 0.75 ± 0.02 | 0.67 ± 0.02 |
| **Sulfate (mg $L^{-1}$)** | 4.85 ± 0.34 | 4.60 ± 0.22 | 4.47 ±0.32 | 4.18 ± 0.17 | 4.60 ± 0.53 |
| **Fluoride (mg $L^{-1}$)** | 2.09 ± 0.32 | 1.49 ± 0.17 | 1.58 ±0.26 | 1.63 ± 0.03 | 1.72 ± 0.22 |
| **Chloride (mg $L^{-1}$)** | 59.71 ± 2.22 | 60.69 ± 1.7 | 60.27 ± 1.65 | 59.39 ± 0.93 | 54.64 ± 7.69 |

## S5 Effect of $TiO_2$-photocatalysis on eukaryotic plankton

**Table S7:** Relative abundance of eukaryotic community (18S rRNA) from the internal assignment considering defined groups for the freshwater systems from the representative taxa obtained after sequencing. Taxa were chosen using 3% of relative abundance threshold at least in one sample. Data are expressed as mean and standard deviation (n=3) as a percentage of the total eukaryotic community.

| Defined groups | Representative taxonomic assignment | T0 | Day 3 | | Day 7 | |
|---|---|---|---|---|---|---|
| | | | Control | $TiO_2$ | Control | $TiO_2$ |
| Diatom | Bacillariophyceae | 1.1 ± 0.8 | 1.2 ± 0.3 | 1.4 ± 0.5 | 0.6 ± 0.3 | 0.3 ± 0.2 |
| | Fragilariales | 9.9 ± 8.2 | 3.9 ± 1.3 | 3.6 ± 1.1 | 5.6 ± 4.2 | 5.4 ± 3.2 |
| | Mediophyceae | 2.1 ± 2.2 | 1.8 ± 0.3 | 2.3 ± 0.5 | 0.8 ± 1 | 1.5 ± 0.9 |
| Chlorophyta | Chlorophyta | 1.6 ± 1.4 | 1.1 ± 0.1 | 1.2 ± 0.5 | 0.4 ± 0.3 | 0.4 ± 0.2 |
| Zooplankton | Podocopa | 2.6 ± 2.7 | 0 ± 0 | 1.8 ± 1.9 | 0 ± 0 | 0 ± 0 |
| | Gastrotricha | 0.8 ± 1.1 | 0 ± 0 | 0 ± 0 | 0.2 ± 0.2 | 0.3 ± 0.4 |
| | Copepoda | 49.9 ± 33.4 | 38.3 ± 10.9 | 35 ± 27.3 | 41.1 ± 14.4 | 4.6 ± 5.4 |
| | Monogononta | 8.3 ± 6 | 15.3 ± 6.9 | 13.6 ± 6.2 | 25.8 ± 13.1 | 1.7 ± 1 |
| Fungi | Blastocladiales | 0.2 ± 0.1 | 0.5 ± 0.1 | 0.6 ± 0.3 | 6.2 ± 2.6 | 0.1 ± 0.1 |
| Alveolate | Dinoflagellata | 4 ± 5.7 | 0.4 ± 0.1 | 0.4 ± 0.2 | 2.4 ± 1 | 1.1 ± 0.5 |
| | Perkinsidae | 1 ± 1 | 1.1 ± 0.1 | 1.1 ± 0.1 | 1.6 ± 1.4 | 8 ± 3.6 |
| | Hypotrichia | 0.6 ± 0.6 | 1.3 ± 0 | 2.1 ± 1.6 | 0.1 ± 0.1 | 0.4 ± 0.2 |
| | Choreotrichia | 0.3 ± 0.3 | 2.5 ± 0.5 | 2.8 ± 2 | 0.4 ± 0.5 | 0 ± 0 |
| Chrysophyte | Chromulinales | 0.5 ± 0.4 | 0.6 ± 0.1 | 0.6 ± 0.2 | 0 ± 0 | 11.7 ± 2.7 |
| | Chrysophyceae | 0.1 ± 0.1 | 0 ± 0 | 0 ± 0 | 0 ± 0 | 10.2 ± 2.1 |
| | Ochromonadales | 0.5 ± 0.6 | 1.5 ± 0.2 | 1.6 ± 0.3 | 0.4 ± 0.6 | 18.9 ± 11.8 |
| Cryptophyte | Cryptophyceae | 3.5 ± 3 | 2.2 ± 0.3 | 2.9 ± 2 | 2.9 ± 2.6 | 1 ± 0.6 |
| Nucleariids | Nucleariidae | 0 ± 0 | 0.1 ± 0 | 0.1 ± 0.1 | 0.1 ± 0 | 6.6 ± 7.1 |
| Eukaryotic_picoplankton_environmental_sample | Eukaryotic_picoplankton_environmental_sample | 0.6 ± 0.5 | 2 ± 0.1 | 2.4 ± 1.4 | 0 ± 0.1 | 0.2 ±0.1 |
| Discicristata_Euglenid | Discicristata | 0.3 ± 0.3 | 3.3 ± 0.6 | 3.6 ± 1.2 | 0.1 ± 0 | 0.2 ± 0.1 |
| | Prokinetoplastina | 0.3 ± 0.3 | 0.2 ± 0 | 0.3 ± 0.1 | 0.3 ± 0.2 | 0.6 ± 0.3 |
| Unclassified | Incertae_Sedis | 0.7 ± 0.4 | 0.8 ± 0.3 | 0.7 ± 0.3 | 4.5 ± 0.4 | 0.5 ± 0.3 |
| | MAST_12C | 0.8 ± 0.6 | 0.7 ± 0.1 | 0.8 ± 0.3 | 0.5 ± 0.1 | 0.2 ± 0.1 |
| Stramenopiles_uncl | Stramenopiles_uncl | 0.7 ± 0.4 | 1.5 ± 0.2 | 1.6 ± 0.4 | 1.1 ± 0.4 | 2 ± 1.8 |
| SAR_uncl | SAR_uncl | 4.1 ± 4.2 | 2.5 ± 0.3 | 2.5 ± 0.8 | 0.6 ± 0.4 | 1.7 ± 0.5 |
| Eukaryota_uncl | Eukaryota_uncl | 5.3 ± 3 | 17.2 ± 1.9 | 17.1 ± 6.9 | 4.2 ± 1.3 | 22.4 ± 1.7 |

## S6 Correlation between plankton and abiotic factors during $TiO_2$-photocatalysis

**Table S8:** Spearman correlation between the main genera, which contributed to the difference between control and treatment according to LEfSe analysis, with physical chemical parameters that showed a difference over the treatment. Spearman r values (threshold r=0.4) are labeled considering a negative (in red) or positive (in green) correlation, from a significant p-value (p<0.05).

| **Bacterioplankton** | | | | | | |
|---|---|---|---|---|---|---|
| **Spearman (p<0.05)** | **Dissolved $O_2$** | **pH** | **Turbidity** | **Transparency** | **TOC** | **DOC** |
| *Armatimonas* | - | - | - | - | - | - |
| *Asinibacterium* | -0.5472 | | -0.73847 | 0.56965 | - | - |
| CL500_3 | - | - | - | - | -0.4663 | - |
| *Cyanobium* | - | - | 0.52406 | -0.60417 | -0.4487 | - |
| *Flectobacillus* | - | -0.5104 | - | - | - | - |
| LD29 | - | - | - | - | -0.5828 | - |
| *Leptolyngbyaceae*_uncl | - | 0.68182 | - | - | - | - |
| *Methylacidiphilaceae*_uncl | - | - | - | - | - | - |
| *Microcystis* | 0.50649 | - | 0.6723 | -0.61068 | - | -0.5301 |
| *Nodosilinea* | - | - | 0.53966 | -0.65886 | - | - |
| *Planktothrix* | 0.4974 | - | 0.6697 | - | - | - |
| *Prochlorothrix* | - | 0.50341 | 0.43447 | - | - | - |
| *Prosthecobacter* | -0.4639 | - | -0.44893 | 0.44104 | 0.61258 | 0.49201 |
| *Raphidiopsis* | - | 0.44156 | 0.54096 | - | - | - |
| *Sphaerospermopsis* | 0.53329 | - | 0.54504 | - | - | - |
| *Terrimicrobium* | - | - | - | - | - | - |
| **Eukaryotes** | | | | | | |
| **Spearman (p<0.05)** | **Dissolved $O_2$** | **pH** | **Turbidity** | **Transparency** | **TOC** | **DOC** |
| *Ploimida* | - | - | - | - | - | - |
| *Calanoida* | - | - | 0.48795 | - | - | -0.5324 |
| *Copepoda_uncl* | - | - | - | - | - | - |
| *Cyclopoida* | - | - | - | -0.54388 | -0.4464 | - |
| *Catenaria* | - | - | - | - | - | - |
| *Ochromonas* | - | - | - | 0.57703 | 0.46833 | 0.58158 |
| *Cryptophyceae*_uncl | - | - | - | - | - | 0.47281 |
| *Poteriospumella* | - | - | -0.44646 | - | - | - |
| *Nuclearia* | -0.4947 | - | -0.63102 | 0.55066 | 0.55506 | 0.53022 |

## S7 Stability of $TiO_2$ coating and post-deployment photocatalytic performance of coated glass beads

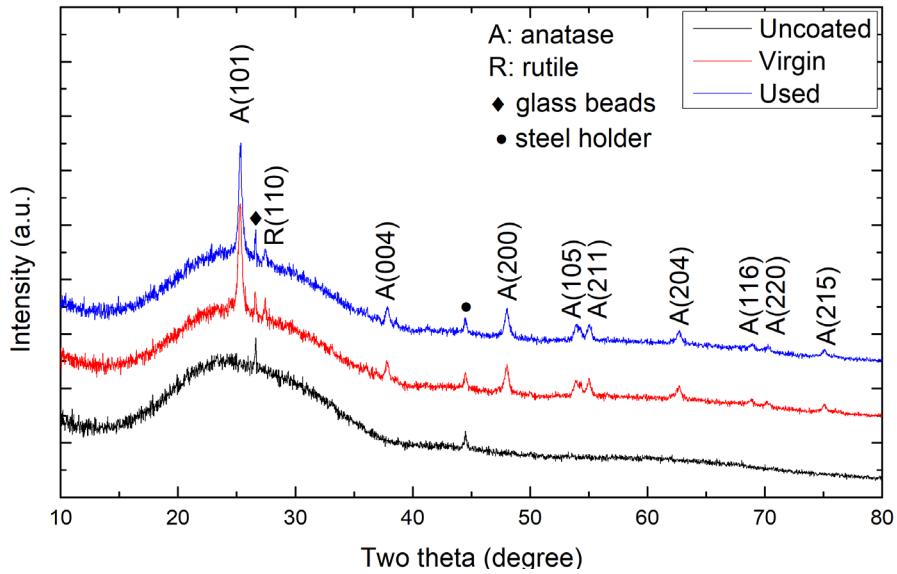


213

214 **Figure S5:** XRD analysis of uncoated, virgin, and used glass beads made from post-

215 consumer glass and coated with $TiO_2$ (virgin and used) showing the stability of the $TiO_2$-

216 coating on the beads.

217

Virgin beads

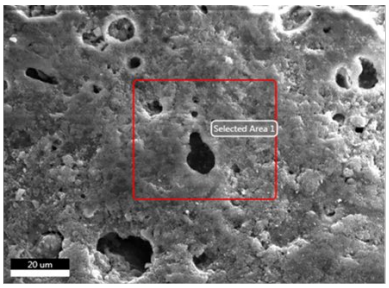


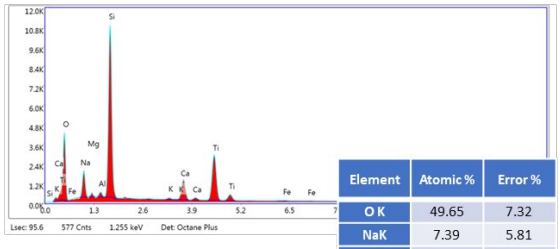

| Element | Atomic % | Error % |
|---|---|---|
| O K | 49.65 | 7.32 |
| Na K | 7.39 | 5.81 |
| Mg K | 0.60 | 11.23 |
| Al K | 0.73 | 7.59 |
| Si K | 25.31 | 2.20 |
| K K | 0.28 | 18.67 |
| Ca K | 4.43 | 2.94 |
| Ti K | 11.45 | 1.83 |
| Fe K | 0.15 | 62.33 |

Used beads


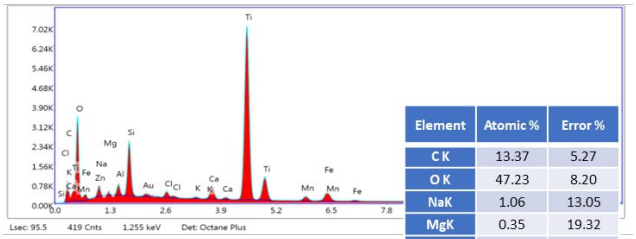

| Element | Atomic % | Error % |
|---|---|---|
| C K | 13.37 | 5.27 |
| O K | 47.23 | 8.20 |
| Na K | 1.06 | 13.05 |
| Mg K | 0.35 | 19.32 |
| Al K | 1.07 | 7.07 |
| Si K | 5.02 | 3.41 |
| Au M | 0.09 | 23.56 |
| Cl K | 0.60 | 13.27 |
| K K | 0.21 | 21.41 |
| Ca K | 1.60 | 4.97 |
| Ti K | 25.49 | 1.70 |
| Mn K | 0.92 | 11.21 |
| Fe K | 2.06 | 6.28 |
| Zn K | 0.93 | 14.25 |

218

**Figure S6:** SEM and EDS analysis of virgin and used $TiO_2$-coated glass beads made from post-consumer glass showing the incorporation of Fe and Mn (from reactor components into the elemental composition) and showing stability of coating.

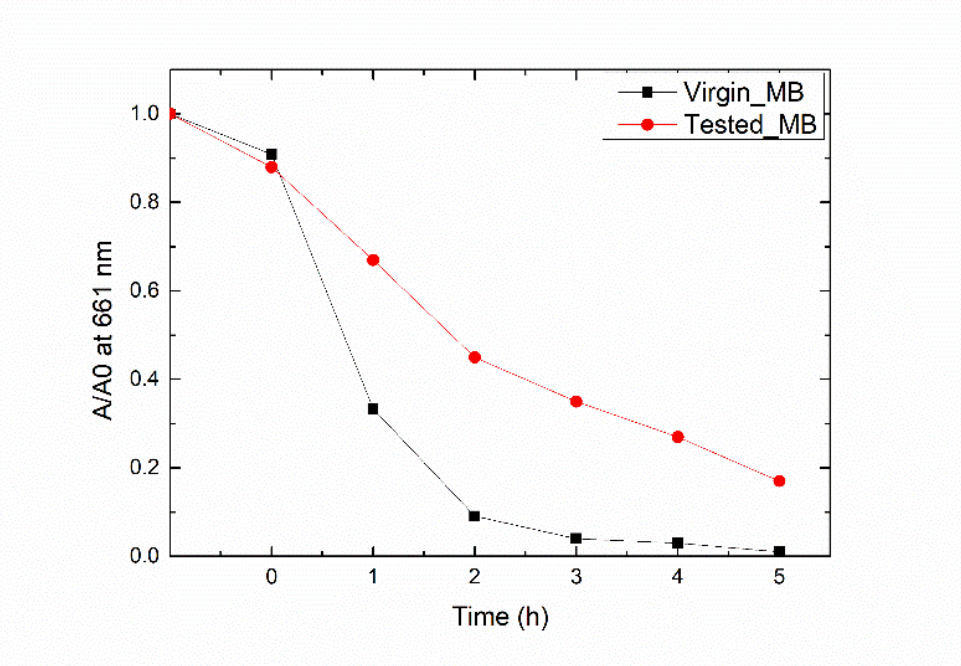


**Figure S7:** Removal of methylene blue by virgin and used (tested) TiO2-coated glass beads made from post-consumer glass using a 250 W iron doped metal halide lamp (λ > 250 nm) at room temperature.

## S8 Preliminary cost analysis of the proposed $TiO_2$-photocatalytic treatment system

Estimation of the cost of a prototype treatment unit is difficult and can be, at best, preliminary. As with any process engineering application cost will need to be determined on a case by case basis. As detailed in the manuscript one of the principles of the *in-situ* concept is that it will be operated over specific periods or continuously to lower the load of cyanobacteria that a water treatment plant will

ultimately need to remove prior to distribution onto the network. As with any process design the overall cost of the process will comprise:

- capital costs,
- fixed costs,
- variable costs,
- operations and maintenance costs.

For this unit the capital/fixed costs will include the cost of the individual treatment pods which comprise the mesh for the unit housing, LED strips and photocatalyst immobilised on the glass beads. As described in the paper the in-situ unit will comprise arrays of these pods depending on the scale of process so the fixed cost of the treatment pods will be dictated by how pods are required. In this study the overall cost for each treatment unit was approximately USD 630 broken down into ~USD 565 for 5 m of water-proof (IP68) 365 nm LED strips with 120 LEDs $m^{-1}$, ~USD 27 for 0.5 $m^2$ of the stainless steel wire mesh to construct the housing and the pods, and an additional ~USD 30 for the aluminium profiles that anchor the LED strips inside of the reactor shell and the water-proof wiring. The raw material cost for the $TiO_2$-coated beads is ~USD 3 for the quantity of beads required for a single reactor.

Again, as detailed in the manuscript, the units may be powered by floating photovoltaic units and this is the other substantial capital cost. The costs of the platform will include costs for:

- Photovoltaic Solar Panels
- Floats to support the PV Panels

- Moorings
- Electrical Cables between panels and to the LEDs in the reactor pods

As the LED arrays use DC there is no requirement for an inverter for this system. In terms of costs of power generated from the floating photovoltaic systems the overall cost per kWh of commercial floating photocaltaic systems are estimated as being between 0.05-0.07 $ kWh. The operational and maintenance costs will again depend on each system and for water treatment systems can vary between 15 and 40% of the overall annual costs and are influenced by a variety of factors such as the scale of the unit.

**References**

Cavalier-Smith, T., 2018. Kingdom Chromista and its eight phyla: a new synthesis emphasising periplastid protein targeting, cytoskeletal and periplastid evolution, and ancient divergences. Protoplasma 255, 297–357. https://doi.org/10.1007/s00709-017-1147-3

Riba, M., Kiss-Szikszai, A., Gonda, S., Parizsa, P., Deak, B., Torok, P., Valko, O., Felfoldi, T., Vasas, G., 2020. Chemotyping of terrestrial *Nostoc* like isolates from alkali grassland area s by non targeted peptide analysis. Algal Res. 46, 101798. https://doi.org/https://doi.org/10.1016/j.algal.2020.101798

Savegnago, R.P., Caetano, S.L., Ramos, S.B., Nascimento, G.B., Schmidt, G.S., Ledur, M.C., Munari, D.P., 2011. Estimates of genetic parameters, and cluster and principal components analyses of breeding values related to egg production traits in a white leghorn population. Poult. Sci. 90, 2174–2188. https://doi.org/10.3382/ps.2011-01474

Segata, N., Izard, J., Waldron, L., Gevers, D., Miropolsky, L., Garrett, W.S., Huttenhower, C., 2011. Metagenomic biomarker discovery and explanation. Genome Biol. 12, 1–18. https://doi.org/10.1186/GB-2011-12-6-R60/FIGURES/6

Simpson, A.G.B., Eglit, Y., 2016. Protist diversification, in: Kliman, R.M. (Ed.), Encyclopedia of Evolutionary Biology Volume 3. Elsevier, Amsterdam, pp. 344–360.

Vaissie, P., Monge, A., Hudsson, F., 2020. Fac toshiny: Perform Factorial Analysis from "FactoMineR" with a Shiny Application. R-package version 2.2.